HHS Public Access

Author manuscript

Sci Signal. Author manuscript; available in PMC 2017 November 10.

Published in final edited form as:

Sci Signal. ; 10(492): . doi:10.1126/scisignal.aal2722.

An engineered S1P chaperone attenuates hypertension and ischemic injury

Steven L. Swendeman[1,2], **Yuquan Xiong**[1,2,*], **Anna Cantalupo**[3,*], **Hui Yuan**[1,2,*], **Nathalie Burg**[3,4], **Yu Hisano**[1,2], **Andreane Cartier**[1,2], **Catherine H. Liu**[3], **Eric Engelbrecht**[1,2], **Victoria Blaho**[3,†], **Yi Zhang**[3], **Keisuke Yanagida**[1,2], **Sylvain Galvani**[1,2], **Hideru Obinata**[5], **Jane E. Salmon**[4], **Teresa Sanchez**[3], **Annarita Di Lorenzo**[3], and **Timothy Hla**[1,2,3,‡]

[1]Vascular Biology Program, Boston Children2019;s Hospital, Boston, MA 02115, USA

[2]Department of Surgery, Harvard Medical School, Boston, MA 02115, USA

[3]Center for Vascular Biology, Department of Pathology and Laboratory Medicine, Weill Cornell Medicine, Cornell University, New York, NY 10065, USA

[4]Hospital for Special Surgery, New York, NY 10021, USA

[5]Gunma University Initiative for Advanced Research, Gunma 371-8511, Japan

Abstract

Endothelial dysfunction, a hallmark of vascular disease, is restored by plasma high-density lipoprotein (HDL). However, a generalized increase in HDL abundance is not beneficial,

‡Corresponding author. timothy.hla@childrens.harvard.edu.
*These authors contributed equally to this work.
†Present address: Sanford Burnham Prebys Research Institute, La Jolla, CA 92037, USA.

SUPPLEMENTARY MATERIALS

www.sciencesignaling.org/cgi/content/full/10/492/eaal2722/DC1

Fig. S1. Sphingolipid base content of purified ApoM-Fc and ApoM-Fc–TM.
Fig. S2. Plasma lipid concentrations in mice after ApoM-Fc administration.
Fig. S3. ApoM-Fc is found in the soluble protein fraction of plasma in vivo.
Fig. S4. ApoM-Fc does not induce lymphopenia.
Fig. S5. ApoM-Fc does not induce lymphocyte accumulation in lymphoid tissues.
Table S1. Physiological variables in mice treated with PBS, ApoM-Fc, or ApoM-Fc–TM.

Author contributions: S.L.S. constructed, expressed, and purified the recombinant proteins; characterized in vitro properties; prepared large-scale preparations for all the studies; analyzed the data; prepared figures; and wrote the manuscript. A.C. conducted the blood pressure experiments and measured plasma nitrite concentrations. Y.X. conducted the cardiac I/R experiments, developed the MEF signaling line, and conducted the signaling experiments using these cells. H.Y. conducted the stroke experiments and analyzed data. N.B. conducted the ECIS experiments and analyzed data. Y.H. developed the HUVEC CRISPR/Cas9 cell line and conducted immunoblot experiments on HUVECs. A.C. conducted the receptor internalization experiments. C.H.L. conducted the in vivo half-life experiments and assisted with mouse experiments. E.E. conducted lymphocyte measurements by flow cytometry. V.B. conducted the blood cell measurement experiments. Y.Z. conducted echocardiography experiments. K.Y. developed the CHO cells used in the signaling experiments. S.G. assisted with in vivo experiments. H.O. designed and expressed the ApoM mutant. J.E.S., T.S., and A.D.L. provided expertise and designed experiments for vascular leak, stroke, and blood pressure studies, respectively. T.H. provided overall direction conceptual input for the project, designed experiments, analyzed data, and wrote the manuscript. All authors contributed to the writing of the manuscript and read the drafts.

Competing interests: Weill Cornell Medicine has filed a patent application [P33974 (7512-01-US)] that describes the development of ApoM-Fc and its uses. The inventors are T.H., S.L.S., A.D.L., and T.S. All other authors declare that they have no competing interests.

Data and materials availability: The reagents described in this manuscript can be obtained through a material transfer agreement from Weill Cornell Medicine and Boston Children’s Hospital.

suggesting that specific HDL species mediate protective effects. Apolipoprotein M–containing HDL ($ApoM^+HDL$), which carries the bioactive lipid sphingosine 1-phosphate (S1P), promotes endothelial function by activating G protein–coupled S1P receptors. Moreover, HDL-bound S1P is limiting in several inflammatory, metabolic, and vascular diseases. We report the development of a soluble carrier for S1P, ApoM-Fc, which activated S1P receptors in a sustained manner and promoted endothelial function. In contrast, ApoM-Fc did not modulate circulating lymphocyte numbers, suggesting that it specifically activated endothelial S1P receptors. ApoM-Fc administration reduced blood pressure in hypertensive mice, attenuated myocardial damage after ischemia/reperfusion injury, and reduced brain infarct volume in the middle cerebral artery occlusion model of stroke. Our proof-of-concept study suggests that selective and sustained targeting of endothelial S1P receptors by ApoM-Fc could be a viable therapeutic strategy in vascular diseases.

INTRODUCTION

Endothelial cell function is essential for normal cardiovascular homeostasis (1, 2). Many environmental and intrinsic risk factors for cardiovascular and cerebrovascular diseases cause endothelial dysfunction. Dysfunctional endothelium is thought to initiate the development of vascular diseases (3). On the other hand, various endogenous factors promote optimal endothelial function and counteract the risk factors (4). One such factor is high-density lipoprotein (HDL), a multifunctional circulating nanoparticle (5).

Numerous epidemiological studies have shown that plasma HDL concentrations are correlated with reduced risk from cardiovascular and cerebrovascular diseases (6, 7) as well as improved outcomes after an ischemic event (8, 9). However, increase of total HDL cholesterol by cholesterol ester transfer protein inhibitors or niacin supplementation does not reduce adverse cardiovascular outcomes (10). In addition, HDL particles are heterogeneous, contain numerous bioactive factors, and regulate vascular, metabolic, and immune functions (11), suggesting that specific HDL particle subtypes regulate unique functions in the cardiovascular system. For example, we have shown that plasma apolipoprotein M–containing HDL ($ApoM^+HDL$) is a physiological carrier of the bioactive lipid sphingosine 1-phosphate (S1P) that acts on G protein (heterotrimeric guanine nucleotide–binding protein)–coupled S1P receptors, suppresses inflammatory responses, and maintains vascular barrier function (12–14). Regarding S1P-dependent immune actions, $ApoM^+HDL$ is not required for lymphocyte egress from secondary lymphoid organs but rather restrains lymphopoiesis in the bone marrow (15). Mice that lack ApoM have alterations in lipoprotein metabolism and exhibit enhanced atherosclerosis in the low-density lipoprotein (LDL) receptor null background. In addition, adenoviral expression of ApoM suppresses atherosclerosis in LDL receptor null mice (16, 17). Plasma ApoM is positively correlated with HDL, LDL, and cholesterol and negatively correlated with acute myocardial infarction, endotoxemia, diabetes, metabolic syndrome, and body mass index (18–21). Together, these observations suggest that $ApoM^+HDL$ promotes endothelial function and that this signaling pathway is compromised in cardiovascular, inflammatory, and metabolic diseases.

The S1P chaperone ApoM contains a lipid-binding pocket that associates with S1P and a tethered signal peptide that allows it to anchor to the HDL particle (22). The binding affinity of S1P to its receptors is higher than that to ApoM, which presumably allows S1P release from the chaperone followed by receptor association and activation (13, 23, 24). Our studies have shown that HDL-bound S1P acts as a "biased agonist" on endothelial $S1P_1$ receptor, which means that only a subset of downstream responses is activated (14). HDL-bound S1P is important for endothelial survival, migration, angiogenesis, nitric oxide (NO) production, and inhibition of inflammatory responses (14, 25–27). In addition, HDL-bound S1P likely engages both an HDL receptor (SR-B1) and S1P receptors to evoke specific biological responses such as stimulation of NO synthesis, inhibition of endothelial injury, and inflammation (28).

Because HDL-bound S1P is limiting under pathophysiological conditions associated with endothelial injury and activation of this pathway promotes endothelial function and restores homeostasis, we devised a strategy to develop a soluble ApoM therapeutic that carries S1P to activate vascular S1P receptors during pathological conditions. In particular, we provide proof-of-concept data that therapeutic restoration of ApoM-bound S1P during hypertensive and ischemic conditions leads to decreased pathologic outcome and/or enhanced recovery from these conditions.

RESULTS

Development of recombinant soluble ApoM to activate S1P receptors

Free ApoM that is not associated with HDL has an extremely short half-life (29). Hence, we developed a strategy to stabilize ApoM in plasma by fusing it with the constant domain (Fc) of immunoglobulins. The ApoM-Fc fusion protein was expressed in both human embryonic kidney (HEK) 293 and insect Sf9 cells, which was efficiently secreted into the conditioned medium. We also prepared an S1P-binding mutant (R98A, W100A, and R116A), referred to as ApoM-Fc–TM (triple mutant), that contained mutations in three amino acid residues that contact the head region of the S1P molecule (Fig. 1A). The purified proteins migrated as oligomers in nonreducing gels but were quantitatively reduced to a 50- to 55-kDa monomer (Fig. 1B). A two-step purification procedure, consisting of concanavalin A affinity chromatography followed by gel filtration chromatography, achieved highly purified ApoM-Fc fusion protein at a yield of 7.8 ± 2.7 μg/ml of conditioned medium. The ApoM-Fc–TM was expressed and purified in a similar manner as the ApoM-Fc fusion protein with a yield of 6.4 ± 1.4 μg/ml. ApoM-Fc, ApoM-Fc–TM, and the immunoglobulin G1 (IgG1)–Fc proteins were purified to homogeneity (Fig. 1C).

The ApoM-Fc bound to S1P with an EC_{50} (effective median concentration) of ~0.22 μM, whereas ApoM-Fc–TM and IgG1-Fc did not show a significant binding activity (Fig. 1D). Further, ApoM-Fc isolated from Sf9 cells contained 1.94 ± 0.31 mole percent (mol %) of S1P, presumably from cells and/or cell culture medium. Very low amounts of sphingosine (0.02 to 0.03 mol %) and dihydrosphingosine (0.04 to 0.06 mol %) were associated with ApoM-Fc and ApoM-Fc–TM (fig. S1), whereas ceramides were not detected. Incubation of ApoM-Fc with S1P (1:8, mol/mol) for 24 to 48 hours at 4°C, followed by purification by gel filtration chromatography, yielded ApoM-Fc containing 51.3 ± 8.1 mol % of S1P (Fig. 1E).

Although purified ApoM-Fc–TM contained only 0.12 ± 0.01 mol % of S1P, it was not increased stoichiometrically after loading with exogenous S1P as above, consistent with the lack of binding of the mutant to S1P. We used S1P-enriched ApoM-Fc for further signaling and biological experiments.

Sustained activation of endothelial cell S1P receptors by S1P-bound ApoM-Fc

Given that ApoM-Fc binds to S1P, we next determined whether it activated S1P receptors. ApoM-Fc activated the β-arrestin–based $S1P_1$ reporter (30) in a dose-dependent manner. Albumin-S1P and ApoM-Fc–TM activated the reporter activity with a similar dose-response relationship (Fig. 2, A and B). In Chinese hamster ovary (CHO) cells expressing $S1P_1$, $S1P_2$, or $S1P_3$, ApoM-Fc but not ApoM-Fc–TM activated phosphorylation of the extracellular signal–regulated kinase (ppERK) (Fig. 2C). ApoM-Fc was more effective than albumin-bound S1P at inducing ppERK in $S1P_1$-expressing CHO cells. In contrast, the effect of ApoM-Fc–TM was negligible (Fig. 2C). In human endothelial cells, ApoM-Fc activated the phosphorylation of ERK, Akt, and endothelial NO synthase (eNOS) (Fig. 2D). In human endothelial cells in which the *S1PR1* or *S1PR3* gene was disrupted with clustered regularly interspaced short palindromic repeats (CRISPR)/CRISPR-associated 9 (Cas9) technology, ApoM-Fc was still effective at inducing ppERK, although it failed to induce ppERK signaling in double knockout cells (Fig. 2E). These data suggest that ApoM-Fc can activate $S1P_1$ and $S1P_3$ receptors in human endothelial cells.

Activation of endothelial cell $S1P_1$ and $S1P_3$ receptors results in the assembly of adherens junctions and the enhancement of barrier function (31), which can be measured by increased transendothelial electrical resistance (TEER). HDL-bound S1P is more potent in promoting vascular barrier function compared to albumin-S1P in vitro and in vivo (12, 13). ApoM-Fc induced a sustained increase in TEER in human umbilical vein endothelial cell (HUVEC) monolayers. Although albumin-bound S1P also enhanced TEER, the effect was transient. In contrast, ApoM-Fc–TM did not increase TEER (Fig. 3A). The ability of ApoM-Fc to increase TEER depended on $S1P_1$ signaling, because it was attenuated in HUVECs that lacked $S1P_1$ by CRISPR/Cas9-mediated gene disruption (Fig. 3B). In addition, although ApoM-Fc induced internalization of $S1P_1$ receptor, the extent of internalization was lower than that induced by FTY720-P, a potent and irreversible inducer of $S1P_1$ endocytosis, or albumin-bound S1P (Fig. 3C). These data suggest that ApoM-Fc induces sustained enhancement of endothelial cell barrier function by activating S1P receptors.

In vivo stability of ApoM-Fc–bound S1P

In vivo stability of ApoM-Fc and ApoM-Fc–TM was determined by measurement of plasma concentrations after intraperitoneal injection. ApoM-Fc and ApoM-Fc–TM showed plasma half-lives of 93.5 and 86.5 hours, respectively, suggesting that they were stable in vivo (Fig. 4A). When 100 μg of ApoM-Fc was injected, plasma S1P and dihydro-S1P concentrations increased by 76.3 ± 13.7% and 52.9 ± 12.9%, respectively, in $Apom^{-/-}$ mice and by 29.9 ± 10.1% and 38.9 ± 4.1%, respectively, in wild-type mice 24 hours thereafter. Plasma concentrations of sphingosine, dihydrosphingosine, ceramides, and cholesterol were unaffected (Fig. 4, B and C, and fig. S2, A and B). Injected ApoM-Fc was not associated with the HDL fraction and was found in the lipoprotein-free fraction (fig. S3). These data

suggest that ApoM-Fc stabilizes bound S1P as a soluble protein in vivo, presumably by protecting it from phosphatase-mediated degradation. We have shown previously that albumin-bound S1P is rapidly degraded in vivo with an estimated half-life of 15 min (32). This property likely explains, at least in part, the sustained biological effects of ApoM-Fc.

In vivo effects of ApoM-Fc–bound S1P on hematopoietic cell trafficking

ApoM-Fc administration and resultant increases in plasma S1P could potentially activate the $S1P_1$ receptor on hematopoietic cells to modulate lymphocyte egress and platelet formation (33, 34). We therefore quantified circulating blood cells after ApoM-Fc administration. Circulating numbers of lymphocytes, white blood cells, platelets, and red blood cells were not altered by ApoM-Fc or ApoM-Fc–TM administration, suggesting that immune and hematopoietic S1P receptors were not activated by ApoM-Fc administration (Fig. 4D). This lack of effect contrasts with the lymphopenia induced by small-molecule $S1P_1$ modulators, which antagonize $S1P_1$ receptors in the secondary lymphoid organs, thymus, and the spleen (33). Flow cytometry analysis to quantify T lymphocyte subsets in circulation and in secondary lymphoid organs confirmed that whereas FTY720 treatment induced marked lymphopenia, ApoM-Fc treatment did not change circulating or lymph node–resident CD4 and CD8 cell numbers (figs. S4, A to D, and S5, A and B). It is likely that ApoM-Fc does not access the $S1P_1$ receptor on hematopoietic cells in lymphoid and/or hematopoietic tissues.

Sustained blood pressure reduction in hypertensive mice after ApoM-Fc administration

Endothelial dysfunction contributes to hypertensive pathophysiology. Plasma S1P modulates vascular tone by stimulating eNOS activity (25, 35), whereas endothelial $S1P_1$ stimulates eNOS activity through the protein kinase Akt (13, 36). We therefore asked whether ApoM-Fc administration modulated blood pressure in hypertensive mice implanted with angiotensin II (AngII) osmotic minipump. In C57BL/6 mice, ApoM-Fc but not ApoM-Fc–TM administration potently reduced blood pressure by ~40 mmHg at 2 hours after treatment (Fig. 5A). The effect of ApoM-Fc was sustained and therapeutic efficacy was maintained for 192 hours after a single dose. This profound and sustained decrease in blood pressure was completely abolished by coadministration with W146, a competitive antagonist for $S1P_1$ (Fig. 5B). In hypertensive mice, plasma nitrite concentrations were increased by ApoM-Fc but not by ApoM-Fc–TM (Fig. 5C). Resting blood pressure in normotensive mice was decreased transiently by ApoM-Fc, but the magnitude and duration were less potent and transient (Fig. 5D). $Apom^{-/-}$ mice showed significantly increased resting blood pressure compared to the wild-type counterparts (Fig. 5E). These data suggest that ApoM-Fc administration activates the endothelial $S1P_1$/eNOS/NO axis to achieve a sustained antihypertensive effect. In contrast to ApoM-Fc, administration of small molecules that target the $S1P_1$ receptor induces a mild increase in blood pressure in rodents and humans, in part because of their functional antagonism of endothelial $S1P_1$ (35, 37).

Effect of ApoM-Fc–bound S1P on cardiac function after myocardial infarction

HDL and S1P suppress ischemia/reperfusion (I/R) injury in rodent and porcine models of myocardial infarction (38–41) and in rodent models of stroke (42, 43). Moreover, therapeutic administration of $S1P_1$ agonists also suppresses I/R injury (44), although a

small-molecule agonist (SEW2871) induces abnormal cardiac rhythm (45, 46). We hypothesized that ApoM-Fc administration would attenuate myocardial ischemia/reperfusion (MI/R) injury due to its protective effect on the endothelium. ApoM-Fc but not ApoM-Fc–TM administration reduced I/R injury at 24 hours after reperfusion (Fig. 6, A and B). In addition, neutrophil accumulation into the infarcted site was attenuated by ApoM-Fc, but vascular density was not altered at the infarcted site, suggesting that ApoM-Fc maintained endothelial homeostasis after MI/R injury (Fig. 6C). Echocardiographic analysis 1 to 2 weeks after I/R injury showed that ApoM-Fc administration significantly preserved myocardial function (Fig. 6, D and E). These data suggest that therapeutic administration of ApoM-Fc activates vascular S1P receptors to suppress MI/R injury.

Effect of ApoM-Fc–bound S1P on brain tissue damage and vascular barrier function after cerebral ischemia

In stroke patients undergoing reperfusion therapies, higher HDL cholesterol concentrations are associated with a favorable outcome at 3 months (8). To investigate the therapeutic potential of ApoM-Fc treatment in cerebral ischemia, we used a mouse model of transient focal cerebral ischemia, the middle cerebral artery occlusion (MCAO) model. After 60 min of ischemia, mice were treated with PBS, ApoM-Fc, or ApoM-Fc–TMat the time of reperfusion. Twenty-three hours after reperfusion, edema and infarct ratios and infarct volumes were calculated as previously described (47). Administration of ApoM-Fc resulted in a decrease in both the infarct size and total edema region, which is the sum of cytotoxic and vasogenic edema (Fig. 7, A to D). Infarct volumes (corrected for edema) were reduced to ~39% in ApoM-Fc–treated mice compared to PBS-treated mice. In contrast, treatment with ApoM-Fc–TM trended toward a protective effect, which did not achieve statistical significance. We also found that the neurological scores were significantly improved in ApoM-Fc–treated mice compared to PBS-treated mice but not in mice treated with ApoM-Fc–TM (Fig. 7E). Cerebral blood flow in the territory of the MCA, which was monitored during the surgeries by laser speckle flowmetry, was similarly reduced in all three groups of mice during occlusion and similarly restored after reperfusion (Fig. 7F). Cerebrovascular permeability, which was assessed by Evans blue dye leakage, was also reduced significantly by ApoM-Fc (Fig. 7G). These data indicate that in an experimental stroke model, ApoM-Fc treatment after reperfusion potently decreases total cerebral edema and infarct size, resulting in improved stroke outcomes. The physiological parameters (arterial oxygen saturation, heart rate, pulse distention, and respiratory rate), measured before, during ischemia, and after reperfusion (47), were not significantly changed in mice treated with PBS, ApoM-Fc, or ApoM-Fc–TM (table S1).

DISCUSSION

S1P is associated with HDL through ApoM, which is tethered to the lipoprotein particle through the N-terminal signal peptide (13). HDL-bound S1P, which accounts for ~5% of total HDL particles, is limiting in various acute and chronic diseases and the animal models that mimic such conditions (18, 44). Under these conditions, supplementation of HDL and $S1P_1$ agonists was beneficial (18, 39). However, HDL infusion is technically challenging (6), and the pharmacological tools suffer from nonspecificity, suboptimal pharmacokinetics,

and off-target effects (37). We hypothesized that therapeutic administration of ApoM-bound S1P would activate vascular S1P receptors and promote endothelial function, thus facilitating the restoration of homeostasis from pathological states.

We developed a novel protein, ApoM-Fc, a soluble factor that binds to S1P. The use of the heterologous signal sequence that is cleaved allowed the processing and secretion along the secretory pathway and efficient release into the extracellular environment. Mutation of key S1P head group–binding residues in the ApoM-Fc–TM protein allowed the discrimination of S1P-dependent actions from other functions of ApoM. The Fc fusion promoted high stability of the protein in vivo. Purified ApoM-Fc bound to S1P with an affinity comparable to that of the native ApoM protein. The association of S1P to ApoM-Fc was stable and survived multiple purification steps. Thus, this novel reagent allowed receptor activation and therapeutic administration in animal models.

ApoM-Fc–bound S1P activated S1P receptors expressed in heterologous cell systems and in endothelial cells. ApoM-Fc–bound S1P activated the $S1P_1$ receptor better than albumin-bound S1P, whereas the effect on $S1P_2$ and $S1P_3$ was similar between the two forms. Moreover, sustained activation of the $S1P_1$ receptor was achieved by ApoM-Fc–bound S1P, resulting in enhancement of endothelial barrier function. This increase in barrier function induced by ApoM-Fc–S1P was more sustained than that induced by albumin-S1P, an effect that could be due to the ability of ApoM-Fc–S1P to induce preferential and chronic signaling of the $S1P_1$ receptor. ApoM-Fc–S1P–treated endothelial cells showed reduced internalization of the $S1P_1$ receptor compared to the albumin-S1P– or FTY720-P–treated endothelial cells. In addition, or alternatively, it is also possible that ApoM-Fc–S1P may be protected from degradative enzymes, thus leading to more sustained signaling.

Pathological hypertension is in part caused by endothelial injury, which leads to enhanced vasoconstrictor responses and attenuated vasodilation (1). S1P activation of endothelial S1P receptors induces eNOS-dependent NO secretion and vasodilation (48). We showed that ApoM-Fc–S1P potently reduced blood pressure in a sustained manner (~190 hours) in AngII-induced hypertensive mice. This effect was completely inhibited by the $S1P_1$ receptor inhibitor and correlated with plasma nitrite concentrations. Because $Apom^{-/-}$ mice showed increased blood pressure when conscious, these data suggest that pharmacological activation of the ApoM-S1P axis could be a strategy to control hypertension.

We presented evidence that ApoM-Fc–S1P suppressed MI/R injury in a mouse model. HDL infusion or $S1P_1$ agonists have been previously shown to protect the myocardium from MI/R injury (38–41). The effect of ApoM-Fc–S1P was associated with reduced infiltration of neutrophils into the myocardium. Thus, restoration of microvascular function in the injured myocardium by ApoM-Fc–S1P could lead to reduced tissue inflammation and injury. Cardiac function was significantly preserved in ApoM-Fc–S1P–treated mice 1 to 2 weeks after myocardial ischemia and injury. We suggest that this strategy may be useful in acute myocardial infarction to preserve endothelial function and promote recovery of the ischemic tissue.

Similarly, ApoM-Fc–S1P administration suppressed neuronal injury in a mouse model of MCAO stroke, which was associated with reduced vascular leak in the affected tissue, suggesting that ApoM-Fc–S1P promoted the function of the blood-brain barrier. In mouse models of stroke, HDL infusion and $S1P_1$ receptor activators can reduce neuronal I/R injury in animal models and in human clinical trials (8, 10, 42, 43, 47, 49, 50). Thus, ApoM-Fc–S1P may provide a novel strategy for treatment of stroke.

The ability to selectively activate vascular S1P receptors with ApoM-Fc recombinant protein provides substantial advantages to small molecules that target this pathway. Small-molecule $S1P_1$ inhibitors are not selective for the vasculature, and short-term agonism evolves into chronic functional antagonism that influences many organ systems (51). Our data show that ApoM-Fc–S1P administration did not lead to lymphopenia, which provides considerable advantage over small-molecule $S1P_1$ agonists.

In summary, we describe the development of a novel, engineered S1P chaperone, ApoM-Fc, which selectively activates vascular S1P receptors in a sustained manner to promote endothelial function and attenuate pathological phenotypes in hypertension and I/R injury of the heart and the brain. Thus, we propose that ApoM-Fc administration could lead to a novel therapy for diseases in which endothelial function is compromised.

MATERIALS AND METHODS

Creation of ApoM-Fc and ApoM-Fc–TM

The ApoM–IgG1-Fc fusion protein was created by cloning a polymerase chain reaction (PCR)–derived complementary DNA (cDNA) corresponding to the Δ_{1-20}ApoM open reading frame (ORF) (52) into the pFUSE-mIgG1-Fc2 vector (InvivoGen; catalog no. pfuse-mg1fc2) between the interleukin-2 signal peptide and the IgG1-Fc framework region. Thus, the 507–base pair (bp) ORF of human ApoM lacking a signal peptide and substituting the stop codon was generated by PCR using the primers 5′-TATCCATGGGGATCTACCAGTGCCCTGAGCACAGT-3′ (forward) and 5′-TATGGATCCTCCGTTATTGGACAGCTCACAGGCCT-3′ (reverse). The forward primer inserts a novel Nco I restriction site (underlined), begins at ApoM codon 21, and eliminates the uncleavable ApoM signal peptide (23). The reverse primer inserts a novel Bam HI restriction site (underlined) and replaced the stop codon (TGA; codon 189) with a glycine codon by an A>G substitution TGA>GGA. The resulting PCR-derived DNA was purified and cleaved by double digestion with Nco I–Bam HI (New England Biolabs; catalog nos. R0193S and R3136S) and ligated (Quick Ligation Kit, New England Biolabs; catalog no. M2200) into the ORF of the pFUSE-mIgG1-Fc2 vector (InvivoGen; catalog no. pfuse-mg1fc2) digested with Nco I–Bgl II (New England Biolabs; catalog nos. R0193S and R0144S). Bgl II is a compatible sticky end for Bam HI and, upon ligation, eliminates both sites. The ligation was transformed into high-efficiency transfection-competent DH5α (Thermo Fisher Scientific; catalog no. 18263012) and selected on Zeocin (25 μg/ml; Thermo Fisher Scientific; catalog no. R25005) Miller’s broth agar petri plates. Individual colonies were picked and grown in 2 ml of Zeocin (25 μg/ml) Miller’s broth, and DNA was isolated using the GeneJET Plasmid Miniprep Kit (Thermo Fisher Scientific; catalog no. K0503). Recombinant vectors were identified using a diagnostic Eco RI (New England Biolabs;

catalog no. R3101S) DNA digest, which releases a 430-bp DNA fragment, and positive clones were sequenced at the Cornell DNA Sequencing Core Facility. This cloning resulted in the fused gene ApoM-Fc (pApoM-Fc). To create a non–S1P-binding negative control for these studies, an ApoM-Fc–TM (pApoM-Fc–TM) was created based on the crystallographic analysis of ApoM (13). Mutations were created by site-directed mutagenesis at codons R98A, W100A, and R116A using the QuikChange II XL Site-Directed Mutagenesis Kit following the manufacturer's protocol and using the primers 5′-CGCCCTG**C**CATG**GC**GACTGAGCTC-3′ (for R98A andW100A) and 5′-AATCATGCTGAATG**C**GACAGGCC-3′ (for R116A). Mutated plasmids were transformed into bacteria as above and selected on Zeocin agar plates. Clones were isolated and subjected to miniprep as above and sequenced as above. This resulted in the mutant fused gene ApoM-Fc–TM (pApoM-Fc–TM).

Expression of ApoM-Fc, ApoM-Fc–TM, and IgG1-Fc proteins in baculovirus

To produce milligram quantities of properly folded, glycosylated protein for in vivo studies, we used the Bac-to-Bac Baculovirus Expression System (Thermo Fisher Scientific/ Invitrogen), which uses recombinant baculovirus to express soluble protein in insect cell supernatant. Using the pApoM-Fc, pApoM-Fc–TM, or the original pFUSE-IgG1-Fc2 (IgG1-Fc alone) plasmids as templates, we performed a further round of PCR using primers reactive to the pFUSE-IgG1-Fc2 vector: 5′-TATGGATCCATGTACAGGATGCAACTCCTGTCTT-3′ (forward) and 5′-TATTTATCATGTCTGGCCAGCTAGCGACACTGGG-3′ (reverse). The forward primer creates a restriction site for Bam HI (underlined), and the reverse primer creates a restriction site for Nhe I (underlined). The resulting PCR-derived DNA cassettes were purified and cleaved by double digestion with Bam HI–Nhe I (New England Biolabs; catalog nos. R3136S and R5131S) and ligated into the baculovirus expression vector pFASTBAC1 (Invitrogen), which was restriction-digested with Bam HI–Xba I (New England Biolabs; catalog nos. R3136S and R5145S). Recombinant viral DNA was generated using the manufacturer's protocol (Invitrogen; Bac-to-Bac Baculovirus Expression System) using DH10BAC *Escherichia coli* bacteria and triple-drug selection using tetracycline (10 μg/ml), gentamicin (7 μg/ml), and kanamycin (50 μg/ml) on LB agar plates. Individual colonies were selected and grown in LB broth supplemented with the same triple-drug combination. Recombinant plasmids were isolated by miniprep as above, and positive clones were sequenced at the Cornell University DNA Sequencing Core Facility. The resulting baculovirus plasmids were termed pApoM-Fc (Bac), pApoM-Fc–TM (Bac), or pIgG1-Fc (Bac).

Production of ApoM-Fc, ApoM-Fc–TM, and IgG1-Fc in HEK293T cells

pApoM-Fc, pApoM-Fc–TM, or the control pFUSE-mIgG1-Fc2 vectors were assayed for protein expression by transfection of HEK293T cells [American Type Culture Collection (ATCC) CRL-1573], using the Lipofectamine 2000 reagent (Thermo Fisher Scientific; catalog no. 11668019). Normal cultures were maintained at 37°C in Dulbecco's modified Eagle's medium (DMEM) supplemented with 10% fetal bovine serum (FBS). Recombinant pApoM-Fc plasmids were transfected into three separate cultures of 293T cells using Lipofectamine 2000 for 72 hours. For the final 18 hours, culture medium was replaced with

serum-free Opti-MEM (Thermo Fisher Scientific; catalog no. 31985-070). Supernatants were collected, clarified by centrifugation, and stored at −80°C until use.

Production of recombinant ApoM-Fc, ApoM-Fc–TM, or IgG1-Fc baculovirus

Recombinant baculoviral DNA (1 to 3 μg) pApoM-Fc (Bac), pApoM-Fc-TM (Bac), or pIgG1-Fc (Bac) was transfected into individual cultures of the insect cell line Sf9 by the calcium phosphate method provided by the manufacturer. After 5 days, the resulting culture supernatant containing viral particles was passaged onto naïve Sf9 cells at a 1:50 dilution and incubated for 5 days. This was repeated three times to create a high-titer viral stock (>10^9 plaque-forming units/ml). For further amplification/maintenance of viral stock, 3 × 10^7 Sf9 cells were seeded into 150-mm^3 tissue culture plates in complete culture medium (Sf900 III) (Thermo Fisher Scientific; catalog no. 12658027), infected with 500 μl of virus suspension from serial viral amplification steps (passage 5), and incubated for 5 days at 27°C. For protein production, 3 × 10^7 High Five (Thermo Fisher Scientific; catalog no. PHG0143) cells were seeded into 150-mm^2 tissue culture plates in complete culture medium (Sf900 III) (Thermo Fisher Scientific; catalog no. 12658027), infected with 1 ml of viral stock, and then incubated for 4 to 5 days at 27°C in a humidified incubator. Supernatants were collected and clarified by centrifugation at 3000*g* for 10 min and stored at 4°C.

Immunoblot analysis of recombinant ApoM-Fc

The identity of the fusion proteins was confirmed using anti-ApoM–specific immunoblot analysis. For most experiments, 10 to 20 μl of the recombinant cell culture supernatant were heated to 95°C for 10 min in 5× Laemmli's sample buffer. Separate samples were prepared either with or without 100 mM dithiothreitol (DTT) (Sigma-Aldrich). Samples were separated on a 12% SDS-PAGE gel (Bio-Rad, Acrylamide; catalog no. 1610156) and transferred electrophoretically to nitrocellulose membrane (Bio-Rad; catalog no. 1620115). Blots were blocked in 5% milk (Carnation) suspended in TBS-T [50 mM tris base (pH 8), 150 mM NaCl, and 0.05% Tween 20] for 1 hour at room temperature (RT) and then incubated with a rabbit anti-ApoM monoclonal antibody (GeneTex GTX62234; clone EPR2904) overnight (>12 hours) and washed with five changes of TBS-T over the course of 30 min. Blots were incubated in 1% milk/TBS-T supplemented with goat anti-rabbit IgG coupled to horseradish peroxidase (HRP) [1:5000 (v/v); Jackson Labs] for 60 min and then washed five times over the course of 30 min in TBS-T at RT with gentle rocking. Blots were incubated with Immobilon Western Chemiluminescent HRP Substrate (Millipore; catalog no. WBKLS0500), and chemiluminescence was revealed using an x-ray film (Denville Scientific, HyBlot CL E3018).

Purification of ApoM-Fc, ApoM-Fc–S1P, ApoM-Fc–TM, and IgG1-Fc

Large-scale purification of fusion proteins was performed on a Bio-Rad NGC FPLC (fast protein liquid chromatography) Chromatography System using the following protocol. In step 1, 100 to 200 ml of the culture supernatant containing the fusion protein were clarified by ultracentrifugation at 42,000 rpm (>100,000*g*; Sorvall Discovery 90, T-1250 Rotor) in sterilized polystyrene screw cap tubes. In step 2, the supernatant was collected and concentrated to $^1/_{10}$ volume using Amicon Ultra-15 Centrifugal filters (Ultracel-50K). In step 3, the concentrated culture supernatant was replaced with 10 volumes of concanavalin A

lectin-binding buffer (LBB) [50 mM tris-HCl (pH 7.5), 300 mM NaCl, 1.5 mM $MnCl_2$, 1 mM $CaCl_2$, and 1 mM $MgCl_2$] in Amicon Ultra-15 Centrifugal filters (Ultracel-50K). In step 4, the protein sample was applied to a 5-ml Bio-Scale MT-5 column of prepacked concanavalin A Sepharose beads previously washed with 20 bed volumes of LBB. The application rate was 0.2 ml/min with an average pressure of 30 psi. In step 5, the column was washed with LBB at a flow rate of 0.4 ml/min until the column flow-through reached buffer baseline OD_{280} (optical density at 280 nm)—typically 55 to 57 milliabsorbance units (mAU). In step 6, proteins were eluted from the column using LBB supplemented with 200 mM α-methyl-mannoside (elution buffer), which was filter-sterilized before use. After subtracting system volume, typically, 2 ml of elution buffer was applied to the column (0.4 ml/min) and then incubated for 15 to 30 min to allow efficient displacement of bound proteins. In step 7, proteins were eluted from the column in elution buffer at a rate of 0.4 ml/min. Fractions (0.8 ml) were collected on a BioFrac collector until the OD_{280} returned to elution buffer baseline (~125 mAU). In step 8, positive fractions were pooled and concentrated 10-fold on an Amicon Ultra-4 Centrifugal Filter (Ultracel-10K), and elution buffer was replaced with 10 volumes of PBS/1 mM EDTA to remove mannose. In step 9, the approximate concentration of fusion protein was determined by bicinchoninic acid protein analysis (Thermo Fisher Scientific) of the sample combined with SDS-PAGE of 5 μg of the preparation. For some experiments, fusion protein was mixed with S1P resuspended in methanol in 1:8 (μmol fusion protein/μmol S1P) and incubated for 24 to 48 hours at 4°C with gentle rocking. The final concentration of methanol in the sample did not exceed 3% (v/v). The sample was concentrated on an Amicon Ultra-4 Centrifugal Filter (Ultracel-10K). In step 10, 1 ml of protein concentrate was injected onto a Superose 6 Increase 10/300 GL column preequilibrated with PBS/1 mM EDTA and separated at a rate of 0.4 ml/min until peak fractions were collected. In step 11, protein positive fractions were pooled and concentrated in an Amicon Ultra-4 Centrifugal Filter (Ultracel-10K). Buffer was replaced with 10 volumes of sterile PBS and maintained at a final concentration of 1 to 3 mg/ml.

Analysis of FPLC protein fractions

All fractions were analyzed by SDS-PAGE. Ten microliters of each fraction was boiled at 95°C in 5× Laemmli's sample buffer supplemented with 100 mM DTT and separated on a 12% SDS-PAGE gel. Gels were fixed in methanol/acetic acid/water (50%:10%:40%) and stained in fixative solution containing 0.3% Coomassie Brilliant Blue (Bio-Rad) and destained in fixative solution.

Measurement of ApoM-Fc binding of S1P based on fluorescence quenching analysis

Previous studies had demonstrated that bacterially expressed recombinant ApoM binds to S1P with a relative affinity of ~1 μM based on fluorescence quenching of Trp^{100} of the predicted human ApoM polypeptide (23). Thus, 0.125, 0.25, and 0.5 μM of ApoM-Fc, ApoM-Fc–TM, or IgG1-Fc were analyzed for lipid-dependent fluorescent quenching on a QuantaMaster 300 (Horiba) collecting emission spectra within the range of 250 to 400 nm. Baseline emission was established, and the emission maxima were determined for each protein sample. For quenching studies, each protein was stabilized for 5 min, and then S1P dissolved in methanol was added to a final concentration of 0.25 to 3.0 μM over the course of 60 min. Because fusion protein was being evaluated and the interest is only in quenching

in ApoM, IgG1-Fc was used as a control for nonspecific quenching of the C terminus of the fusion protein. Emission fluorescence of IgG1-Fc was subtracted from all appropriate ApoM-Fc and ApoM-Fc–TM data. Data were collected and analyzed using FelixGX software.

Measurement of S1P in purified ApoM-Fc, ApoM-Fc–TM, or blood plasma after injection of ApoM fusion proteins

Fifty micrograms of purified ApoM-Fc, ApoM-Fc–S1P, ApoM-Fc–TM, or ApoM-Fc–TM was analyzed for sphingolipid content by LC–mass spectrometry (LC-MS) at the Stony Brook University Lipidomics Core Facility. For plasma studies, *Apom*$^{-/-}$ or C57BL/6 mice were pre-bled by the cheek punch method and allowed to rest for 24 to 48 hours. Mice were injected intraperitoneally with 100 μg (4 mg/kg) of ApoM-Fc–S1P or ApoM-Fc–TM, and after 24 hours, blood was collected in EDTA and centrifuged at 2000*g* for 10 min to collect plasma. Twenty-five micro-liters of plasma was analyzed for sphingolipid content and species by LC-MS.

In vitro analysis of S1P-dependent signal transduction in $S1P_1$ reporter cells

Kono *et al.* have established a mouse strain based on the β-arrestin signaling to record $S1P_1$ signaling (called the $S1P_1$-GFP signaling mouse) (30). Essentially, activation of the $S1P_1$ receptor by S1P results in accumulation of a histone-GFP fusion protein in the nuclei of activated cells. We established a MEF line from day 10.5 embryos. With standard protocols, embryos were dissociated, and MEFs were isolated and transformed with SV40 large T antigen. The resulting transformed cells were selected for low endogenous GFP expression and maintained in DMEM supplemented with 10% charcoal-stripped FBS, which contains very low amounts of S1P. For functional assays, we determined that the addition of fatty acid–free (FAF) albumin-S1P results in nuclear GFP accumulation, appearing as early as 6 hours with maximum signal at 24 hours after stimulus. Treated cells were harvested by trypsinization and directly analyzed by fluorescence-activated cell sorting (FACS) analysis, gating on GFP expression. With this assay, 0.12 to 1 μM of ApoM-Fc–S1P or ApoM-Fc–TM were assayed for $S1P_1$ activation and GFP expression by FACS analysis. Data were expressed as % GFP-positive/total live cells analyzed.

Analysis of the effect of ApoM-Fc or ApoM-Fc–TM on signal transduction through $S1P_1$ to $S1P_3$

We previously reported the analysis of $S1P_1$ signaling in stably transfected CHO cells using $S1P_1$ cDNA cloned into the lentiviral vector p (CHO-$S1P_1$) (13). We established separate CHO cell clones for $S1P_2$ using the Tet-On vector system (CHO-$S1P_2$) and $S1P_3$ using the pcDNA3.1 Edg3 (cDNA Resource Center). Cells were maintained in Ham's F12 medium (Invitrogen) supplemented with 10% FBS. For analysis of signal transduction, seeded cultures were allowed to adhere overnight, washed twice in serum-free medium, and then cultured overnight in medium supplemented with 0.1% FAF-albumin. Medium was replaced, and cells were incubated for 5, 15, and 30 min with Opti-MEM alone or albumin-S1P (100 nM S1P), ApoM-Fc–S1P (100 nM S1P), or ApoM-Fc–TM (12 μg/ml). Alternatively, cells were subjected to a dose response with albumin-S1PorApoM-Fc–S1P diluted to 0, 25, 50, 100, or 200 nM S1P or ApoM-Fc–TM(12 μg/ml). Cells were washed

briefly with PBS and then lysed in PBS/NP-40 [PBS, 1%NP-40, protease inhibitors (Sigma), and 1 mM $NaVO_3$, 10 mM NaF, and 10 mM β-glycerol phosphate]. Lysates were clarified by centrifugation for 10 min at 4°C at 13,000*g*, and supernatants were mixed with 5× Laemmli's buffer containing 100 mM DTT. Samples were separated on a 12% SDS-PAGE gel (Bio-Rad, Acrylamide; catalog no. 1610156) and transferred electrophoretically to nitrocellulose membrane (Bio-Rad; catalog no. 1620115). Blots were blocked in 5% milk (Carnation) suspended in TBS-T [50 mM tris base (pH 8), 150 mM NaCl, and 0.05% Tween 20] for 1 hour at RT and then incubated with a mouse monoclonal antibody for phospho-p44/42 mitogen-activated protein kinase (MAPK) (Thr^{202}/Tyr^{204}) [(E10) 9106S, Cell Signaling] at 1:1000 overnight (>12 hours) and washed with five changes of TBS-T over the course of 30 min. Blots were incubated in 1% milk/TBS-T supplemented with goat anti-mouse IgG coupled to HRP (1:5000; The Jackson Laboratory) for 60 min and then washed five times over the course of 30 min in TBS-T at RT with gentle rocking. Blots were incubated with Immobilon Western Chemiluminescent HRP Substrate (Millipore; catalog no. WBKLS0500), and chemiluminescence was revealed using an x-ray film (Denville Scientific, HyBlot CL E3018). To confirm equal loading, blots were stripped using glycine (pH 2.5) for 10 min and reprobed with rabbit anti-ERK1/2 (Santa Cruz Biotechnology; catalog no. sc-292838). Blots were incubated, washed, and developed as described above.

HUVECs (ATCC 100-010) were maintained in supplemented EGM buffer and split before assay. Cells were starved in 0.1% FAF-albumin medium for 4 hours and then assayed. For signaling experiments, starved cells were cultured at 5, 15, or 30 min with albumin-S1P (100 to 400 nM S1P), ApoM-Fc–S1P (5 to 20 μg/ml), or ApoM-Fc–TM (5 to 20 μg/ml). Cells were lysed, and lysates were separated and transferred for Western blotting of phospho-p44/42 MAPK as described above. Blots were stripped and reprobed for expression of pAkt (Ser^{473}) (Cell Signaling; catalog no. 9271L) and total Akt (Cell Signaling; catalog no. 9272S). Blots were incubated, washed, and developed as described above. Immunoblots were analyzed for activation of phospho-eNOS (Ser^{1177}) (Cell Signaling; catalog no. 9571S) and total eNOS abundance (BD Biosciences; catalog no. 610296).

Generation of $S1P_1$-, $S1P_3$-, and $S1P_{1/3}$ double knockout HUVEC by CRISPR/Cas9

Guide RNA (gRNA) targeting the *S1PR1* starting codon was designed and cloned into the lentiCRISPRv2 vector (a gift from F. Zhang; Addgene plasmid #529619) (53) using the following oligonucleotides: 5′-CACCGCGGGACGCTGGTGGGCCCCA-3′ and 5′-AAACTGGGGCCCACCAGCGTCCCGC-3′. gRNA targeting *S1PR3* included 5′-caccgGAGGGCAGTTGCCATCACT-3′ and 5′-aaacAGTGATGGCAACTGCCCTCc-3′, 5′-caccgAACCGCATGTACTTTTTCAT-3′ and 5′-aaacATGAAAAAGTACATGCGGTTc-3′, 5′-caccgCTTCTGCATCAGCATCTTCA-3′ and 5′-aaacTGAAGATGCTGATGCAGAAGc-3′, and 5′-caccgCATGGCACTGCTGCGGACCG-3′ and 5′-aaacCGGTCCGCAGCAGTGCCATGc-3′.

Lentiviral particles were prepared using HEK293T cells and infected into HUVECs. Forty-eight hours after infection, puromycin (2 μg/ml) was added for selection, HUVECs were analyzed for the mutation of the *S1PR1* or *S1PR3* locus by DNA sequencing, and $S1P_1$

protein expression was determined by immunoblot analysis. $S1P_3$ expression was determined by quantitative PCR analysis.

Measurement of $S1P_1$ internalization

U2OS human osteosarcoma cells that stably expressed the $S1P_1$ receptor fused to GFP were generated and selected for high-level expression. Cells were plated in a 384-well plate and brought to confluence. Cells were then starved in serum-free medium for 2 hours, and individual wells were stimulated for 30 min with indicated concentrations of FTY720-P, albumin-S1P (10 to 100 nM), ApoM-Fc–S1P (1 to 20 μg/ml), or ApoM-Fc–TM (1 to 20 μg/ml). Cells were then fixed for 15 min with 4% paraformaldehyde (PFA) and permeabilized for 10 min in PBS/0.1% Triton. Nuclei were stained with DAPI for 5 min. Cells were maintained in PBS and imaged in 384-well plates by an ArrayScan VTI at ×10 using the spot detector software.

Measurement of endothelial cell barrier function in vitro

HUVECs were maintained as described before (13) and analyzed between passages 4 and 8. Endothelial barrier function was evaluated by measuring the resistance of a cell-covered electrode by using an endothelial cell impedance system (ECIS) instrument (Applied BioPhysics). HUVECs were plated on 0.1% fibronectin-coated electrodes (8W10E plates) at a density of 1×10^5 cells per well. Confluent cells were starved for 2 to 6 hours in endothelial basal medium (EBM-2; Lonza) and treated with either albumin-S1P (50 to 200 nM; Sigma-Aldrich), ApoM-Fc–S1P, or ApoM-Fc–TM (both 0.2 to 0.4 μM). Resistance was monitored and expressed as fractional resistance, normalizing to the baseline at the initiation of the assay.

Mice and cell lines

C57BL/6 male mice (6 to 8 weeks old) were purchased from The Jackson Laboratory. ApoM knockout mice in the C57BL/6 background were maintained as previously reported (13). All animal protocols were approved by the Institutional Animal Care and Use Committee of Weill Cornell Medicine and conducted at that institution. All cell lines were tested for mycoplasma contamination.

Measurement of the plasma half-life of ApoM-Fc or ApoM-TM in C57BL/6 mice

Four C57BL/6 mice (6 to 8 weeks old) were administered (intraperitoneally) 100 μg (4 mg/kg) of either purified ApoM-Fc or ApoM-Fc–TM and analyzed at 2, 4, 6, 8, 24, 48, 72, 96, 120, 168, and 216 hours after injection. One microliter of plasma was analyzed by SDS-PAGE and anti-ApoM immunoblot analysis as described above. Ponceau S staining was performed to establish that loading per lane was equivalent. Scans of Western blots were quantified for protein abundance by ImageJ analysis using uninjected plasma as a control. Maximum signal was observed between 4 and 6 hours, which was used as the reference point for evaluating abundance at various time points.

Effect of ApoM-Fc administration on blood cell counts in wild-type mice

C57BL/6 wild-type mice were injected with 100 μg (4 mg/kg) of ApoM-Fc–S1P, ApoM-Fc–TM, or PBS by intraperitoneal injection. After either 6 or 24 hours, blood was harvested into 2 mM EDTA, and the cellular fractions were separated by centrifugation. Total blood cell counts were determined by clinical cytometry (Cytometry Core, Memorial Sloan Kettering Cancer Center).

Analysis of lymphocyte counts by flow cytometry after ApoM-Fc administration

C57BL/6 mice (8 to 10 weeks old) were injected intraperitoneally with either PBS ($n = 5$), ApoM-Fc (4 mg/kg; $n = 5$), ApoM-Fc–TM(4 mg/kg; $n = 5$), or FTY720 (0.5 mg/kg; $n = 5$) (Cayman Chemical). After 18 hours, mice were exsanguinated, and blood was collected in 25 μl of EDTA and maintained on ice. Four hundred microliters of whole blood was centrifuged at 2000*g* for 15 min, and plasma was removed and stored at −20°C. Cells were then subjected to erythrocyte lysis, washed with PBS, and fixed for 30 min in 0.1% PFA–PBS. Cells were washed and stained for flow cytometry. Single-cell suspensions were created from spleen and lymph nodes (two inguinal and brachial lymph nodes per mouse) by gently disaggregating the tissue between frosted glass slides. Spleen cells were then washed with 1% FBS in PBS, and red blood cells were lysed as before. After another PBS wash, samples were gently fixed with 0.1% PFA for 30 min and then washed with 1% FBS in PBS.

After fixation, cells were washed with 1% FBS in PBS [flow buffer (FB)], and Fc receptors were blocked with anti-CD16/32 (eBioscience). Cells were then aliquoted and stained in antibody cocktails for 30 min on ice. After washing with FB, liquid counting beads (BD Biosciences) were added to each sample, and data were obtained on BDLSR II (Becton Dickson) and analyzed using FlowJo software (Tree Star Inc.).

Antibodies used were as follows: phycoerythrin–anti-mouse CD4 (BioLegend), allophycocyanin (APC)–anti-mouse CD8a monoclonal antibody (53-6.7; eBioscience), and APC–Cyanine7–anti-mouse CD3e (17A2; Thermo Fisher Scientific). Data analysis was performed using Prism software.

Analysis of the effect of ApoM-Fc and ApoM-Fc–TM on systolic blood pressure in normotensive mice

Systolic, diastolic, and mean blood pressure was measured in conscious 12-week-old male mice using the pneumatic tail-cuff method (MRBP System, Life Science). Briefly, animals were placed in a plastic chamber maintained at 34°C, and a cuff with a pneumatic pulse sensor was attached to the tail. After 1 week of training, multiple measurements were performed per mouse, and the values were averaged. Mice were given intraperitoneal injections of PBS (vehicle control), ApoM-Fc–S1P, or ApoM-Fc–TM (4 mg/kg), and blood pressure was monitored at 1, 2, 4, 8, and 24 hours and then every 24 hours until day 7.

Chronic infusion of AngII and analysis of the effect of ApoM-Fc and ApoM-Fc–TM on hypertension

AngII (500 ng/kg per minute) was infused using an osmotic minipump (model ALZET 2004) as described previously (35). Briefly, minipumps were implanted subcutaneously in

C57BL/6 (wild-type) male mice at 10 weeks of age. Blood pressure was monitored twice per week from days 0 to 14 of AngII infusion. Systolic blood pressure was evaluated as described above. In another set of experiments, C57BL/6 mice were treated by intraperitoneal injection with PBS (vehicle control) or 100 μg (4 mg/kg) of either ApoM-Fc or ApoM-Fc–TM suspended in PBS, and blood pressure was measured at different time points (1 to 216 hours) after injection. To determine dose-response relationships, a similar experiment was performed using PBS (vehicle control) or 30 μg (1.3 mg/kg) of either ApoM-Fc or ApoM-Fc–TM suspended in PBS. In addition, the $S1P_1$ antagonist W146 (10 mg/kg) (8) was used in similar experiments. W146 was administered by intraperitoneal injection at time 0 and then at 24-hour intervals (24 to 96 hours and then again at 168 hours).

Measurement of plasma nitrite in AngII-treated mice after ApoM-Fc–S1P or ApoM-Fc–TM

NO concentrations were measured as nitrite in plasma from AngII-treated wild-type mice 72 hours after infusion with ApoM-Fc–S1P or ApoM-Fc–TM, using a modified Griess reaction as described previously (35). Briefly, after precipitation of plasma proteins with $ZnSO_4$ (30%, w/v), supernatants were chemically reduced with acid-washed (0.24 M HCl) cadmium powder (Sigma-Aldrich). After centrifugation, samples were measured for nitrite content with Griess reagent (0.1% naphtylethylendiamine dihydrochloride in H_2O and 1% sulfanilamide in 5% concentrated H_3PO_4) and read at a wavelength of 550 nm. All samples were assayed in duplicate, and the NO concentration was calculated against a $NaNO_2$ calibration curve.

MI/R in vivo

We used a model for MI/R injury as previously reported (54). Essentially, the thoracic cavity of anesthetized mice was opened by a small incision between the ribs to expose the heart. The left anterior descending artery of the heart was compressed by a slipknot suture ligation. After 45 min, the slipknot was removed and the incision was closed. After 24 hours, the mice were sacrificed. To visualize the AAR, the heart was perfused with Alcian blue dye through the aorta and coronary arteries and the extent of infarction was evaluated by microscopic analysis of 1-mm transverse sections of the heart. The heart was counterstained with 1% TTC solution for 15 min. Images were visualized by light microscopy and photographed. The infarct area and the AAR (non-blue) and the total left ventricle were evaluated after ImageJ analysis and expressed as the percentage of infarcted area as follows: (no Alcian blue perfusion)/total cardiac area below the suture ligation (55). For all experiments, 30 min before surgery, wild-type C57BL/6 mice were dosed with 100 μl intravenously by retro-orbital injection with ApoM-Fc–S1P (4 mg/kg) or ApoM-Fc–TM (4 mg/kg).

Immunofluorescence staining and histological analysis of MI/R

Twenty-four hours after I/R, mice were sacrificed and hearts were perfused with cold PBS, fixed in 4% PFA for 24 hours, and then embedded in the OCT compound (Sakura Finetek). Cryosections (10 μm thick) were cut and stained with primary antibodies against Ly6G(BioLegend; catalog no. 108401) and biotin-conjugated IsolectinGS-IB4 (Invitrogen; catalog no. I21414). Cy3-conjugated streptavidin (Invitrogen) and fluorescein

isothiocyanate–conjugated anti-rat antibody were used as secondary reagents. Images were visualized by confocal microscopy using an Olympus FluoView FV10i.

Echocardiographic studies

Cardiac dimensions and function were analyzed by transthoracic echocardiography using a Vevo 770 Imaging System (VisualSonics). Mice were lightly anesthetized with inhaled isoflurane (0.2% in O_2). Left ventricle M-mode was used, all measurements were obtained from three to six consecutive cardiac cycles, and the average values were used for analysis. LVDd and LVDs dimensions were measured from the M-mode traces, and fractional shortening was calculated as follows: [(LVDd − LVDs)/LVDd]. Diastolic measurements were taken at the point of maximum cavity dimension, and systolic measurements were made at the point of minimum cavity dimension, using the leading-edge method of the American Society of Echocardiography (56).

Transient MCAO and treatments

Transient focal cerebral ischemia was induced in mice by MCAO as we have previously described (tMCAO) (47). Thirty-three mice (male, 24 to 28g; C57BL/6) were used in this study. The criterion for exclusion was the development of subarachnoid hemorrhage. No animals were excluded from this study. Surgeries and all behavioral and histological assessments were performed by an investigator blinded to the drug treatment. Mice were anesthetized with 3% isoflurane vaporized in O_2 for induction and 1.5% isoflurane for maintenance. Temperature was maintained at 36.5° ± 0.5°C, controlled by a thermostatic blanket (CMA 450 Temperature Controller for mice, Harvard Apparatus) throughout the procedure. The left common carotid artery was exposed, and the occipital artery branches of the external carotid artery (ECA) were isolated and coagulated. The ECA was dissected distally and coagulated along with the terminal lingual and maxillary artery branches. The internal carotid artery (ICA) was isolated, and the extracranial branch of the ICA was then dissected. A rubber silicone-coated monofilament suture (filament size, 6-0; diameter, 0.09 to 0.11 mm; length, 20 mm; diameter with coating, 0.23 ± 0.02 mm; coating length, 5 mm; Doccol Corp.) was introduced into the ECA lumen through an incision and then gently advanced about 9 to 9.5 mm in the ICA lumen to block MCA blood flow. For reperfusion, the suture was withdrawn 60 min after MCAO. 2D laser speckle flowmetry (PeriCam PSI HR, Perimed) was used to confirm MCAO and reperfusion. Right after removal of the suture, animals randomly received an intraperitoneal injection of PBS, ApoM-Fc, or ApoM-Fc–TM.

Physiological parameters (arterial O_2 saturation, heart rate, pulse distention, and respiratory rate) were recorded before, during, and after tMCAO using the MouseOx Plus (Starr Life Sciences Corp.). After the surgery, all animals were maintained in a small-animal heated recovery chamber (IMS Vetcare Chamber Recovery Unit, Harvard Apparatus). After recovery, animals were returned to their cages with free access to food and water. The mortality rate was 1/11 in PBS-treated mice, 0/11 in ApoM wild-type mice, and 1/11 in ApoM-TM–treated mice.

Neurobehavioral testing

Neurological function was evaluated at 23 hours after reperfusion. Neurological deficit was graded on a score of 0 to 4 as previously described (57–59): 0, no observable deficit; 1, forelimb flexion; 2, forelimb flexion and decreased resistance to lateral push; 3, forelimb flexion, decreased resistance to lateral push, and unilateral circling; and 4, forelimb flexion and being unable or difficult to ambulate.

TTC staining and determination of infarct and edema ratios and infarct volumes

Twenty-three hours after reperfusion, mice were anesthetized and decapitated. The brain was quickly removed from cranium, placed in a −20°C freezer for 20 min, and then cut into 1.5-mm coronal slices using a rodent brain matrix. Sections were stained with 2% TTC (Sigma Co.) at 37°C for 10 min and then scanned. Infarct area on each slice was determined by using ImageJ analysis software (National Institutes of Health, Bethesda, MD) to obtain the infarct ratios, edema ratios, and infarct volumes per brain (in cubic millimeters). Infarct areas were calculated by using the following equation to correct for edema formation in the ischemic hemisphere (60): $I = X - Y$, where X is the area of the contralateral (non-ischemic) hemisphere and Y is the area of the intact regions of the ipsilateral (ischemic) hemisphere. Infarct ratios were obtained after normalization by the contralateral hemisphere. Edema ratios were calculated with the following formula: $E = (Z - X)/X$, where Z is the area of the ipsilateral hemisphere.

Statistical analyses, randomization, and blinding for brain studies

All values reported are means ± SEM. P values were calculated with GraphPad Prism software, using one-way nonparametric ANOVA (Kruskal-Wallis) followed by Dunn's test. The criterion for statistical significance was set at $P < 0.05$. All animal experiments used randomization to treatment groups and blinded assessment (61).

Other statistical analyses

All statistical analyses were performed with Prism version 4.03 (GraphPad Software Inc.). Groups of two were compared by using two-tailed Student's t test. Where appropriate, Welch's correction for unequal variances was applied. ANOVA (one-way or two-way) was performed as indicated with either Tukey's post hoc test or Bonferroni's test for multiple comparisons. $P \leq 0.05$ indicated statistical significance.

Supplementary Material

Refer to Web version on PubMed Central for supplementary material.

Acknowledgments

We thank D. Zurakowski for advice on biostatistics; D. Eliezer for help with fluorescence spectroscopy; I. Mileva for sphingolipid measurements; J. Sadoshima for help with MI/R studies; F. Zhang for the lentiCRISPRv2 vector; R. Nachman, D. Falcone, and L. Steinman for comments; and C. Yun and D. Kahler for technical support and analysis for the receptor internalization assays. **Funding:** This work was supported by NIH grants (HL89933, HL117798, HL135821, and HL67330 to T.H.; HL126913 to A.D.L.; and HL094465 to T.S.), a Transatlantic network grant from the Fondation Leducq to T.H. and T.S., and American Heart Association grant 12GRNT12050110 to T.S. The NYU High Throughput Biology Core was supported by the Laura and Isaac

Perlmutter Cancer Center Support Grant (NIH/NCI P30CA16087) and NYSTEM contract no. C026719. Y.H. and K.Y. were supported in part by postdoctoral fellowships from the Japan Society for the Promotion of Science Overseas Research Fellowships. Y.H. was also supported by the Uehara Memorial Foundation.

References

1. Harrison DG. Endothelial dysfunction in atherosclerosis. Basic Res. Cardiol. 1994; 89(suppl. 1):87–102. [PubMed: 7945179]
2. Pober JS, Sessa WC. Evolving functions of endothelial cells in inflammation. Nat. Rev. Immunol. 2007; 7:803–815. [PubMed: 17893694]
3. Girouard H, Iadecola C. Neurovascular coupling in the normal brain and in hypertension, stroke, and Alzheimer disease. J. Appl. Physiol. 2006; 100:328–335. [PubMed: 16357086]
4. Libby P, Ridker PM, Hansson GK. Leducq Transatlantic Network on Atherothrombosis, Inflammation in atherosclerosis: From pathophysiology to practice. J. Am. Coll. Cardiol. 2009; 54:2129–2138. [PubMed: 19942084]
5. Rosenson RS, Brewer HB Jr, Ansell BJ, Barter P, Chapman MJ, Heinecke JW, Kontush A, Tall AR, Webb NR. Dysfunctional HDL and atherosclerotic cardiovascular disease. Nat. Rev. Cardiol. 2016; 13:48–60. [PubMed: 26323267]
6. Hovingh GK, Rader DJ, Hegele RA. HDL re-examined. Curr. Opin. Lipidol. 2015; 26:127–132. [PubMed: 25692348]
7. Rader DJ, Tall AR. The not-so-simple HDL story: Is it time to revise the HDL cholesterol hypothesis? Nat. Med. 2012; 18:1344–1346. [PubMed: 22961164]
8. Makihara N, Okada Y, Koga M, Shiokawa Y, Nakagawara J, Furui E, Kimura K, Yamagami H, Hasegawa Y, Kario K, Okuda S, Naganuma M, Toyoda K. Effect of serum lipid levels on stroke outcome after rt-PA therapy: SAMURAI rt-PA registry. Cerebrovasc. Dis. 2012; 33:240–247. [PubMed: 22261711]
9. Olsson AG, Schwartz GG, Szarek M, Sasiela WJ, Ezekowitz MD, Ganz P, Oliver MF, Waters D, Zeiher A. High-density lipoprotein, but not low-density lipoprotein cholesterol levels influence short-term prognosis after acute coronary syndrome: Results from the MIRACL trial. Eur. Heart J. 2005; 26:890–896. [PubMed: 15764620]
10. Keene D, Price C, Shun-Shin MJ, Francis DP. Effect on cardiovascular risk of high density lipoprotein targeted drug treatments niacin, fibrates, and CETP inhibitors: Meta-analysis of randomised controlled trials including 117,411 patients. BMJ. 2014; 349:g4379. [PubMed: 25038074]
11. Rye K-A, Bursill CA, Lambert G, Tabet F, Barter PJ. The metabolism and anti-atherogenic properties of HDL. J. Lipid Res. 2009; 50:S195–S200. [PubMed: 19033213]
12. Christensen PM, Liu CH, Swendeman SL, Obinata H, Qvortrup K, Nielsen LB, Hla T, Di Lorenzo A, Christoffersen C. Impaired endothelial barrier function in apolipoprotein M–deficient mice is dependent on sphingosine-1-phosphate receptor 1. FASEB J. 2016; 30:2351–2359. [PubMed: 26956418]
13. Christoffersen C, Obinata H, Kumaraswamy SB, Galvani S, Ahnström J, Sevvana M, Egerer-Sieber C, Muller YA, Hla T, Nielsen LB, Dahlbäck B. Endothelium-protective sphingosine-1-phosphate provided by HDL-associated apolipoprotein M. Proc. Natl. Acad. Sci. U.S.A. 2011; 108:9613–9618. [PubMed: 21606363]
14. Galvani S, Sanson M, Blaho VA, Swendeman SL, Obinata H, Conger H, Dahlbäck B, Kono M, Proia RL, Smith JD, Hla T. HDL-bound sphingosine 1-phosphate acts as a biased agonist for the endothelial cell receptor $S1P_1$ to limit vascular inflammation. Sci. Signal. 2015; 8:ra79. [PubMed: 26268607]
15. Blaho VA, Galvani S, Engelbrecht E, Liu C, Swendeman SL, Kono M, Proia RL, Steinman L, Han MH, Hla T. HDL-bound sphingosine-1-phosphate restrains lymphopoiesis and neuroinflammation. Nature. 2015; 523:342–346. [PubMed: 26053123]
16. Wolfrum C, Poy MN, Stoffel M. Apolipoprotein M is required for preβ-HDL formation and cholesterol efflux to HDL and protects against atherosclerosis. Nat. Med. 2005; 11:418–422. [PubMed: 15793583]

17. Christoffersen C, Jauhiainen M, Moser M, Porse B, Ehnholm C, Boesl M, Dahlbäck B, Nielsen LB. Effect of apolipoprotein M on high density lipoprotein metabolism and atherosclerosis in low density lipoprotein receptor knock-out mice. J. Biol. Chem. 2008; 283:1839–1847. [PubMed: 18006500]
18. Frej C, Linder A, Happonen KE, Taylor FB, Lupu F, Dahlbäck B. Sphingosine 1-phosphate and its carrier apolipoprotein M in human sepsis and in *Escherichia coli* sepsis in baboons. J. Cell. Mol. Med. 2016; 20:1170–1181. [PubMed: 26990127]
19. Borup A, Christensen PM, Nielsen LB, Christoffersen C. Apolipoprotein M in lipid metabolism and cardiometabolic diseases. Curr. Opin. Lipidol. 2015; 26:48–55. [PubMed: 25551802]
20. Nielsen LB, Christoffersen C, Ahnström J, Dahlbäck B. ApoM: Gene regulation and effects on HDL metabolism. Trends Endocrinol. Metab. 2009; 20:66–71. [PubMed: 19200746]
21. Plomgaard P, Dullaart RPF, De Vries R, Groen AK, Dahlbäck B, Nielsen LB. Apolipoprotein M predicts pre-β-HDL formation: Studies in type 2 diabetic and nondiabetic subjects. J. Intern. Med. 2009; 266:258–267. [PubMed: 19457058]
22. Axler O, Ahnström J, Dahlbäck B. Apolipoprotein M associates to lipoproteins through its retained signal peptide. FEBS Lett. 2008; 582:826–828. [PubMed: 18279674]
23. Sevvana M, Kassler K, Ahnström J, Weiler S, Dahlbäck B, Sticht H, Muller YA. Mouse ApoM displays an unprecedented seven-stranded lipocalin fold: Folding decoy or alternative native fold? J. Mol. Biol. 2010; 404:363–371. [PubMed: 20932978]
24. Lee M-J, Van Brocklyn JR, Thangada S, Liu CH, Hand AR, Menzeleev R, Spiegel S, Hla T. Sphingosine-1-phosphate as a ligand for the G protein-coupled receptor EDG-1. Science. 1998; 279:1552–1555. [PubMed: 9488656]
25. Nofer J-R, van der Giet M, Tölle M, Wolinska I, von Wnuck Lipinski K, Baba HA, Tietge UJ, Gödecke A, Ishii I, Kleuser B, Schäfers M, Fobker M, Zidek W, Assmann G, Chun J, Levkau B. HDL induces NO-dependent vasorelaxation via the lysophospholipid receptor $S1P_3$. J. Clin. Invest. 2004; 113:569–581. [PubMed: 14966566]
26. Nofer J-R, Levkau B, Wolinska I, Junker R, Fobker M, von Eckardstein A, Seedorf U, Assmann G. Suppression of endothelial cell apoptosis by high density lipoproteins (HDL) and HDL-associated lysosphingolipids. J. Biol. Chem. 2001; 276:34480–34485. [PubMed: 11432865]
27. Kimura T, Tomura H, Mogi C, Kuwabara A, Damirin A, Ishizuka T, Sekiguchi A, Ishiwara M, Im D-S, Sato K, Murakami M, Okajima F. Role of scavenger receptor class B type I and sphingosine 1-phosphate receptors in high density lipoprotein-induced inhibition of adhesion molecule expression in endothelial cells. J. Biol. Chem. 2006; 281:37457–37467. [PubMed: 17046831]
28. Sato K, Okajima F. Role of sphingosine 1-phosphate in anti-atherogenic actions of high-density lipoprotein. World J. Biol. Chem. 2010; 1:327–337. [PubMed: 21537467]
29. Faber K, Hvidberg V, Moestrup SK, Dahlbäck B, Nielsen LB. Megalin is a receptor for apolipoprotein M, and kidney-specific megalin-deficiency confers urinary excretion of apolipoprotein M. Mol. Endocrinol. 2006; 20:212–218. [PubMed: 16099815]
30. Kono M, Tucker AE, Tran J, Bergner JB, Turner EM, Proia RL. Sphingosine-1-phosphate receptor 1 reporter mice reveal receptor activation sites in vivo. J. Clin. Invest. 2014; 124:2076–2086. [PubMed: 24667638]
31. McVerry BJ, Garcia JGN. Endothelial cell barrier regulation by sphingosine 1-phosphate. J. Cell. Biochem. 2004; 92:1075–1085. [PubMed: 15258893]
32. Venkataraman K, Lee Y-M, Michaud J, Thangada S, Ai Y, Bonkovsky HL, Parikh NS, Habrukowich C, Hla T. Vascular endothelium as a contributor of plasma sphingosine 1-phosphate. Circ. Res. 2008; 102:669–676. [PubMed: 18258856]
33. Cyster JG, Schwab SR. Sphingosine-1-phosphate and lymphocyte egress from lymphoid organs. Annu. Rev. Immunol. 2012; 30:69–94. [PubMed: 22149932]
34. Zhang L, Orban M, Lorenz M, Barocke V, Braun D, Urtz N, Schulz C, von Brühl M-L, Tirniceriu A, Gaertner F, Proia RL, Graf T, Bolz S-S, Montanez E, Prinz M, Müller A, von Baumgarten L, Billich A, Sixt M, Fässler R, von Andrian UH, Junt T, Massberg S. A novel role of sphingosine 1-phosphate receptor S1pr1 in mouse thrombopoiesis. J. Exp. Med. 2012; 209:2165–2181. [PubMed: 23148237]

35. Cantalupo A, Zhang Y, Kothiya M, Galvani S, Obinata H, Bucci M, Giordano FJ, Jiang X-C, Hla T, Di Lorenzo A. Nogo-B regulates endothelial sphingolipid homeostasis to control vascular function and blood pressure. Nat. Med. 2015; 21:1028–1037. [PubMed: 26301690]
36. Igarashi J, Michel T. S1P and eNOS regulation. Biochim. Biophys. Acta. 2008; 1781:489–495. [PubMed: 18638569]
37. Camm J, Hla T, Bakshi R, Brinkmann V. Cardiac and vascular effects of fingolimod: Mechanistic basis and clinical implications. Am. Heart J. 2014; 168:632–644. [PubMed: 25440790]
38. Morel S, Christoffersen C, Axelsen LN, Montecucco F, Rochemont V, Frias MA, Mach F, James RW, Naus CC, Chanson M, Lampe PD, Nielsen MS, Nielsen LB, Kwak BR. Sphingosine-1-phosphate reduces ischaemia-reperfusion injury by phosphorylating the gap junction protein Connexin43. Cardiovasc. Res. 2016; 109:385–396. [PubMed: 26762268]
39. Sattler K, Gräler M, Keul P, Weske S, Reimann CM, Jindrová H, Kleinbongard P, Sabbadini R, Bröcker-Preuss M, Erbel R, Heusch G, Levkau B. Defects of high-density lipoproteins in coronary artery disease caused by low sphingosine-1-phosphate content: Correction by sphingosine-1-phosphate-loading. J. Am. Coll. Cardiol. 2015; 66:1470–1485. [PubMed: 26403344]
40. Theilmeier G, Schmidt C, Herrmann J, Keul P, Schäfers M, Herrgott I, Mersmann J, Larmann J, Hermann S, Stypmann J, Schober O, Hildebrand R, Schulz R, Heusch G, Haude M, von Wnuck Lipinski K, Herzog C, Schmitz M, Erbel R, Chun J, Levkau B. High-density lipoproteins and their constituent, sphingosine-1-phosphate, directly protect the heart against ischemia/reperfusion injury in vivo via the $S1P_3$ lysophospholipid receptor. Circulation. 2006; 114:1403–1409. [PubMed: 16982942]
41. Santos-Gallego CG, Vahl TP, Goliasch G, Picatoste B, Arias T, Ishikawa K, Njerve IU, Sanz J, Narula J, Sengupta PP, Hajjar RJ, Fuster V, Badimon JJ. Sphingosine-1-phosphate receptor agonist fingolimod increases myocardial salvage and decreases adverse postinfarction left ventricular remodeling in a porcine model of ischemia/reperfusion. Circulation. 2016; 133:954–966. [PubMed: 26826180]
42. Lapergue B, Dang BQ, Desilles J-P, Ortiz-Munoz G, Delbosc S, Loyau S, Louedec L, Couraud P-O, Mazighi M, Michel J-B, Meilhac O, Amarenco P. High-density lipoprotein–based therapy reduces the hemorrhagic complications associated with tissue plasminogen activator treatment in experimental stroke. Stroke. 2013; 44:699–707. [PubMed: 23422087]
43. Wei Y, Yemisci M, Kim H-H, Yung LM, Shin HK, Hwang S-K, Guo S, Qin T, Alsharif N, Brinkmann V, Liao JK, Lo EH, Waeber C. Fingolimod provides long-term protection in rodent models of cerebral ischemia. Ann. Neurol. 2011; 69:119–129. [PubMed: 21280082]
44. Levkau B. HDL-S1P: Cardiovascular functions, disease-associated alterations, and therapeutic applications. Front. Pharmacol. 2015; 6:243. [PubMed: 26539121]
45. Hofmann U, Burkard N, Vogt C, Thoma A, Frantz S, Ertl G, Ritter O, Bonz A. Protective effects of sphingosine-1-phosphate receptor agonist treatment after myocardial ischaemia-reperfusion. Cardiovasc. Res. 2009; 83:285–293. [PubMed: 19416991]
46. Tsukada YT, Sanna MG, Rosen H, Gottlieb RA. S1P1-selective agonist SEW2871 exacerbates reperfusion arrhythmias. J. Cardiovasc. Pharmacol. 2007; 50:660–669. [PubMed: 18091583]
47. Kim GS, Yang L, Zhang G, Zhao H, Selim M, McCullough LD, Kluk MJ, Sanchez T. Critical role of sphingosine-1-phosphate receptor-2 in the disruption of cerebrovascular integrity in experimental stroke. Nat. Commun. 2015; 6:7893. [PubMed: 26243335]
48. Cantalupo A, Di Lorenzo A. S1P signaling and de novo biosynthesis in blood pressure homeostasis. J. Pharmacol. Exp. Ther. 2016; 358:359–370. [PubMed: 27317800]
49. Fu Y, Zhang N, Ren L, Yan Y, Sun N, Li Y-J, Han W, Xue R, Liu Q, Hao J, Yu C, Shi F-D. Impact of an immune modulator fingolimod on acute ischemic stroke. Proc. Natl. Acad. Sci. U.S.A. 2014; 111:18315–18320. [PubMed: 25489101]
50. Zhu Z, Fu Y, Tian D, Sun N, Han W, Chang G, Dong Y, Xu X, Liu Q, Huang DR, Shi F-D. Combination of the immune modulator fingolimod with alteplase in acute ischemic stroke: A pilot trial. Circulation. 2015; 132:1104–1112. [PubMed: 26202811]
51. Hla T, Brinkmann V. Sphingosine 1-phosphate (S1P): Physiology and the effects of S1P receptor modulation. Neurology. 2011; 76:S3–S8.

52. Xu N, Dahlbäck B. A novel human apolipoprotein (apoM). J. Biol. Chem. 1999; 274:31286–31290. [PubMed: 10531326]

53. Sanjana NE, Shalem O, Zhang F. Improved vectors and genome-wide libraries for CRISPR screening. Nat. Methods. 2014; 11:783–784. [PubMed: 25075903]

54. Xu Z, Alloush J, Beck E, Weisleder N. A murine model of myocardial ischemia-reperfusion injury through ligation of the left anterior descending artery. J. Vis. Exp. 2014:51329.

55. Shao D, Zhai P, Del Re DP, Sciarretta S, Yabuta N, Nojima H, Lim D-S, Pan D, Sadoshima J. A functional interaction between Hippo-YAP signalling and FoxO1 mediates the oxidative stress response. Nat. Commun. 2014; 5:3315. [PubMed: 24525530]

56. Zhang Y, Huang Y, Cantalupo A, Azevedo PS, Siragusa M, Bielawski J, Giordano FJ, Di Lorenzo A. Endothelial Nogo-B regulates sphingolipid biosynthesis to promote pathological cardiac hypertrophy during chronic pressure overload. JCI Insight. 2016; 1:e85484. [PubMed: 27158676]

57. Menzies SA, Hoff JT, Betz AL. Middle cerebral artery occlusion in rats: A neurological and pathological evaluation of a reproducible model. Neurosurgery. 1992; 31:100–106. [PubMed: 1641086]

58. Belayev L, Alonso OF, Busto R, Zhao W, Ginsberg MD. Middle cerebral artery occlusion in the rat by intraluminal suture. Neurological and pathological evaluation of an improved model. Stroke. 1996; 27:1616–1623. [PubMed: 8784138]

59. Mokudai T, Ayoub IA, Sakakibara Y, Lee E-J, Ogilvy CS, Maynard KI. Delayed treatment with nicotinamide (vitamin B_3) improves neurological outcome and reduces infarct volume after transient focal cerebral ischemia in Wistar rats. Stroke. 2000; 31:1679–1685. [PubMed: 10884473]

60. Swanson RA, Morton MT, Tsao-Wu G, Savalos RA, Davidson C, Sharp FR. A semiautomated method for measuring brain infarct volume. J. Cereb. Blood Flow Metab. 1990; 10:290–293. [PubMed: 1689322]

61. Lapchak PA, Doyan S, Fan X, Woods CM. Synergistic effect of AJW200, a von Willebrand factor neutralizing antibody with low dose (0.9 mg/mg) thrombolytic therapy following embolic stroke in rabbits. J. Neurol. Neurophysiol. 2013; 4:146.

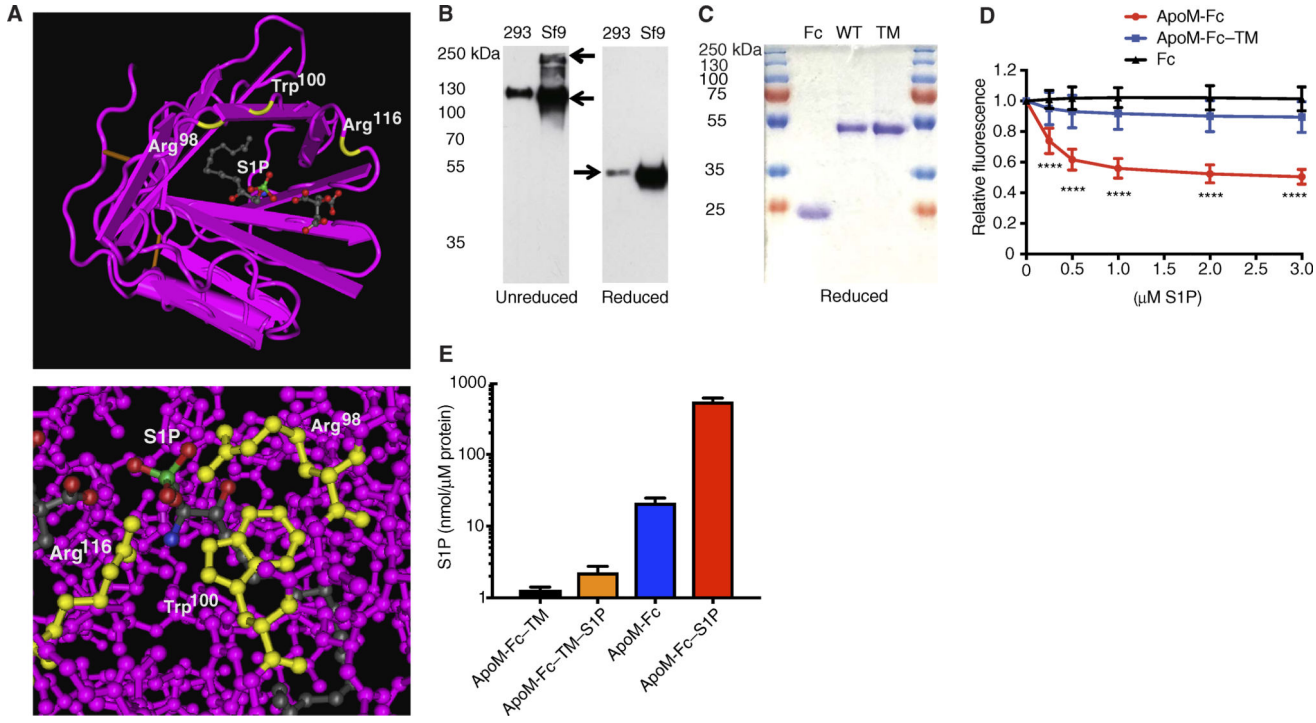

Fig. 1. Production, purification, and characterization of S1P binding by ApoM-Fc and ApoM-Fc–TM fusion proteins

(**A**) Top: Cocrystal structure of S1P bound to ApoM. Three residues (Arg^{98}, Trp^{100}, and Arg^{116}) that contact the phosphate head group region of S1P (red and green) are labeled in yellow. Bottom: Space-filling model of the head group region of S1P in the ApoM molecule. (**B**) ApoM-Fc and ApoM-Fc–TM fusion proteins in the conditioned medium of HEK293 or Sf9 cells were separated by nonreducing or reducing 10% SDS–polyacrylamide gel electrophoresis (PAGE) and detected by anti-ApoM antibody. (**C**) Sf9-derived purified proteins (4 μg) were analyzed by reducing 10% SDS-PAGE and stained with Coomassie Brilliant Blue. WT, wild type. (**D**) Purified IgG1-Fc (Fc), ApoM-Fc, or ApoM-Fc–TM (TM) was analyzed for S1P binding by fluorescence spectrofluorimetry as described ($n = 4$ independent experiments; mean ± SD). ****$P < 0.001$, Student's t test and two-way analysis of variance (ANOVA) followed by Dunnett's posttest comparing ApoM-Fc or ApoM-Fc–TM to Fc alone (ApoM-Fc and ApoM-Fc–TM). (**E**) Purified ApoM-Fc and ApoM-Fc–TM (5 μM) were incubated or not with S1P as described for 24 to 48 hours, purified by gel filtration chromatography, and analyzed for sphingolipids by electrospray ionization–MS/MS. The resulting data are expressed as means ± SD; $n = 4$ independent experiments.

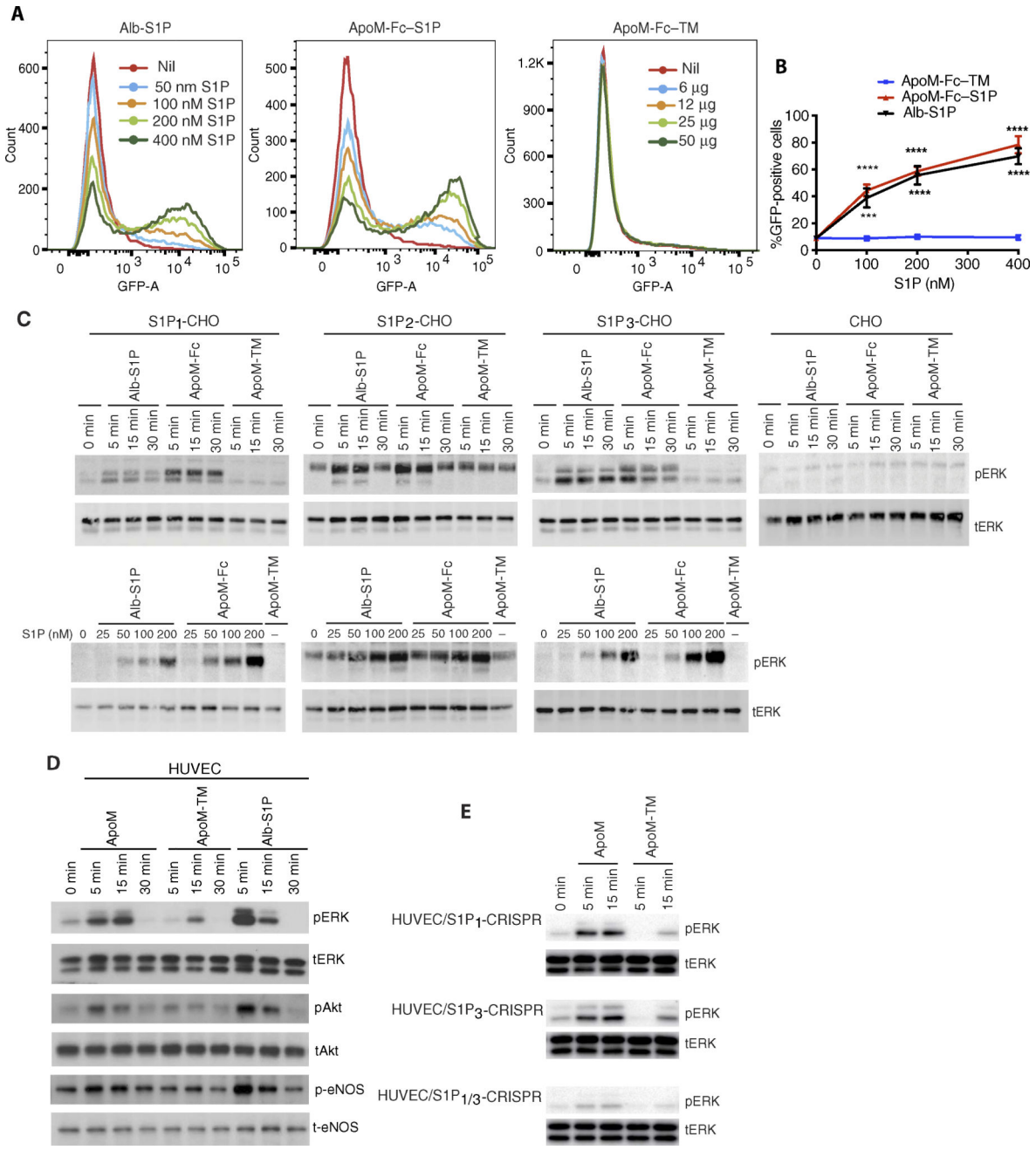

Fig. 2. ApoM-Fc activates S1P receptors

(**A**) Increasing doses of albumin (Alb)–S1P, ApoM-Fc, or ApoM-Fc–TM were incubated with mouse embryonic fibroblasts (MEFs) isolated from $S1P_1$–green fluorescent protein (GFP) signaling mice for 24 hours and analyzed by flow cytometry. S1P and protein concentrations are indicated. (**B**) Quantitative analysis of results from (A). $n = 3$ independent experiments; mean ± SD. ***$P < 0.01$, ****$P < 0.001$, two-way ANOVA followed by Tukey's posttest comparing ApoM-Fc or Alb-S1P to ApoM-Fc–TM. (**C**) CHO cells or CHO cells stably transduced with $S1P_1$, $S1P_2$, or $S1P_3$ were treated for 5 to 30 min using albumin-S1P, ApoM-Fc–S1P (both 100 nM S1P), or ApoM-Fc–TM (12 µg/ml) (top) or by a dose

response with albumin-S1P or ApoM-Fc–S1P diluted to 0 to 200 nM S1P or ApoM-Fc–TM (12 μg/ml) (bottom). Samples were analyzed for phospho-p44/42 ERK (pERK) and total p42/44 ERK (tERK) by immunoblotting. (**D**) HUVECs were treated with albumin-S1P (333 nM S1P), ApoM-Fc–S1P (20 μg/ml; 240 nM S1P) (ApoM), or ApoM-Fc–TM (20 μg/ml) for indicated times and analyzed by immunoblotting for activation of p44/42 ERK, Akt, and eNOS. (**E**) CRISPR/Cas9-derived $S1P_1$, $S1P_3$, or $S1P_{1/3}$ knockout (KO) HUVECs were treated with ApoM-Fc–S1P (12 μg/ml; 100 nM S1P) and analyzed by immunoblotting for activation of p44/42 ERK. $n = 3$ independent experiments with a representative blot shown.

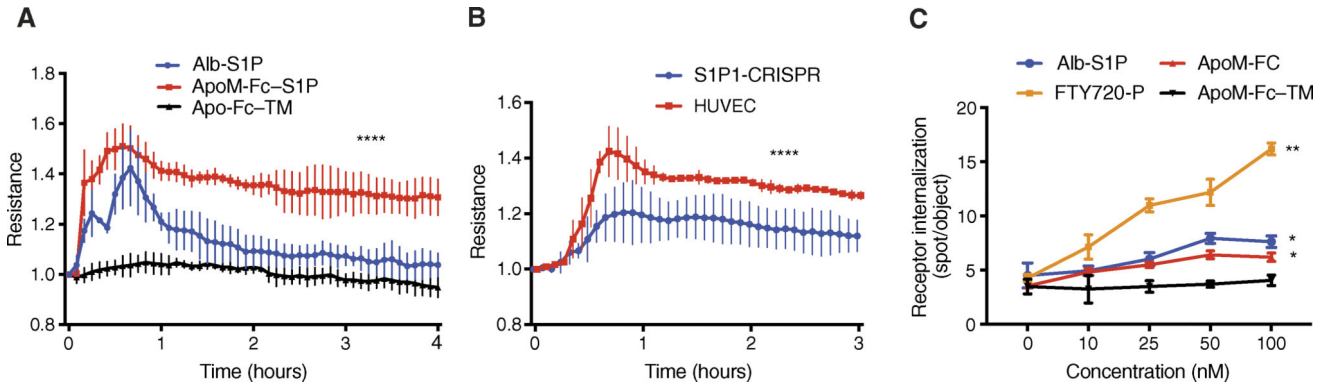

Fig. 3. Effect of ApoM-Fc on endothelial cell barrier function and S1P receptor endocytosis

(**A**) HUVECs were analyzed for barrier function by real-time measurement of TEER. At time 0, either albumin-S1P (200 nM), ApoM-Fc (20 μg/ml; 200 nM S1P), or ApoM-Fc–TM (20 μg/ml) was added. All data were compared to baseline ApoM-Fc–TM. $n = 3$ independent experiments; expressed as mean ± SEM. ****$P < 0.0001$, two-way ANOVA followed by t test. (**B**) HUVECs or $S1P_1$ KO HUVECs ($S1P_1$-CRISPR) were treated with ApoM-Fc (10 μg/ml; 100 nM S1P) and analyzed for barrier function by real-time measurement of TEER. ****$P < 0.0001$, one-way ANOVA followed by t test. $n = 3$ independent experiments. (**C**) U2OS cells expressing $S1P_1$-GFP were treated with indicated concentrations of FTY720-P, Alb-S1P, ApoM-Fc, or ApoM-Fc–TM for 30 min at 37°C. Receptor internalization was quantified. All data were compared to baseline ApoM-Fc–TM. $n = 2$ independent experiments, $n = 8$ wells analyzed in total; expressed as mean ± SEM. **$P < 0.01$, *$P < 0.05$, t test; $P < 0.01$, one-way ANOVA.

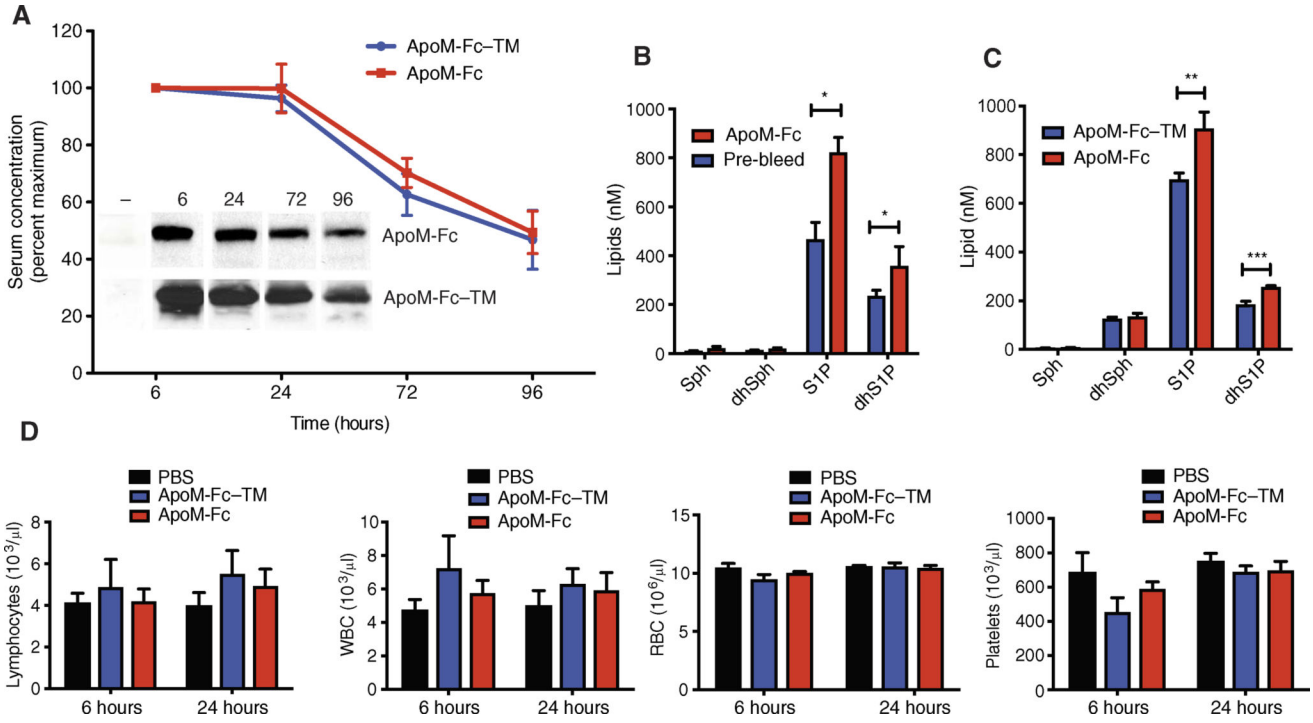

Fig. 4. Effect of ApoM-Fc administration on plasma S1P concentrations and circulating hematopoietic cells

(**A**) WT mice were treated with purified ApoM-Fc (4 mg/kg) or ApoM-Fc–TM (4 mg/kg) (n = 4 mice per treatment) by intraperitoneal injection, and plasma ApoM concentrations were determined by immunoblot analysis. (**B**) *Apom*$^{-/-}$ mice (n = 4 mice; expressed as mean ± SD) were administered ApoM-Fc–S1P (4 mg/kg), and plasma sphingolipids at 24 hours after administration were quantified. Sph, sphingosine; dhSph, dihydrosphingosine. (**C**) WT mice (n = 4 mice per treatment; expressed as mean ± SD) were administered purified ApoM-Fc–S1P (4 mg/kg) or ApoM-Fc–TM (4 mg/kg) by intraperitoneal injection, and plasma sphingolipids at 24 hours after administration were quantified. (B and C) *P = 0.05; **P < 0.01; ***P < 0.005, two-tailed Student's t test. (**D**) WT mice were administered either phosphate-buffered saline (PBS) (n = 5 mice), purified ApoM-Fc–S1P (4 mg/kg) (n = 5 mice), or ApoM-Fc–TM (4 mg/kg) (n = 5 mice) by intraperitoneal injection, and blood was collected at 6 and 24 hours after injection. Blood cells were isolated by centrifugation, and lymphocytes, white blood cells (WBCs), red blood cells (RBCs), and platelets were quantified as described. The observed variations in relative blood cells counts were statistically insignificant as judged by two-way ANOVA and Tukey's posttest. For ApoM-Fc, N.S. was P > 0.55 (lymphocytes), P > 0.33 (WBCs), P > 0.07 (platelets), and P > 0.15 (RBCs).

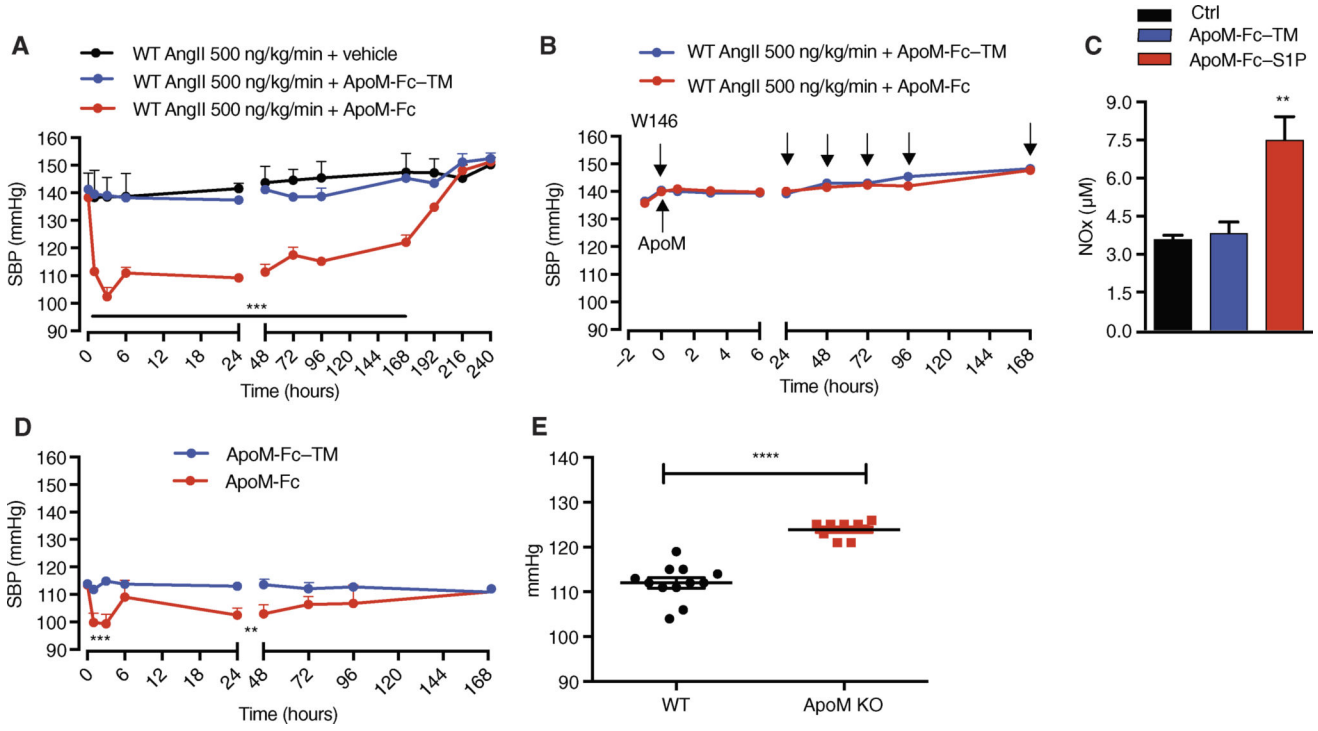

Fig. 5. ApoM-Fc administration leads to a sustained antihypertensive effect in mice

(**A**) Systolic blood pressure (SBP) was measured at the indicated times in AngII-treated WT mice administered with either vehicle (PBS) ($n = 5$ mice), ApoM-Fc (4 mg/kg) ($n = 7$ mice), or ApoM-Fc–TM (4 mg/kg) ($n = 4$ mice) by intraperitoneal injection. (**B**) AngII-treated mice were injected with either ApoM-Fc or ApoM-Fc–TM and the $S1P_1$ antagonist W146 (10 mg/kg) every 24 hours (arrows) followed by measurement of SBP ($n = 5$ mice per treatment). (**C**) ApoM-Fc or ApoM-Fc–TM was administered to AngII-treated mice ($N = 6$ mice per treatment) for 72 hours, and plasma nitrite concentrations were measured as described. (**D**) SBP was measured in normotensive mice administered with either ApoM-Fc (4 mg/kg) ($n = 6$ mice) or ApoM-Fc–TM (4 mg/kg) ($n = 4$ mice) by intraperitoneal injection. (**E**) SBP was measured in WT ($n = 12$ mice) or *Apom*$^{-/-}$ ($n = 11$ mice) mice as described. All data are expressed as means ± SEM. $^{**}P < 0.01$; $^{***}P < 0.005$; $^{****}P < 0.001$ compared to WT (A to D). Statistical significance was determined by two-way ANOVA followed by Bonferroni's post hoc test or one-way ANOVA.

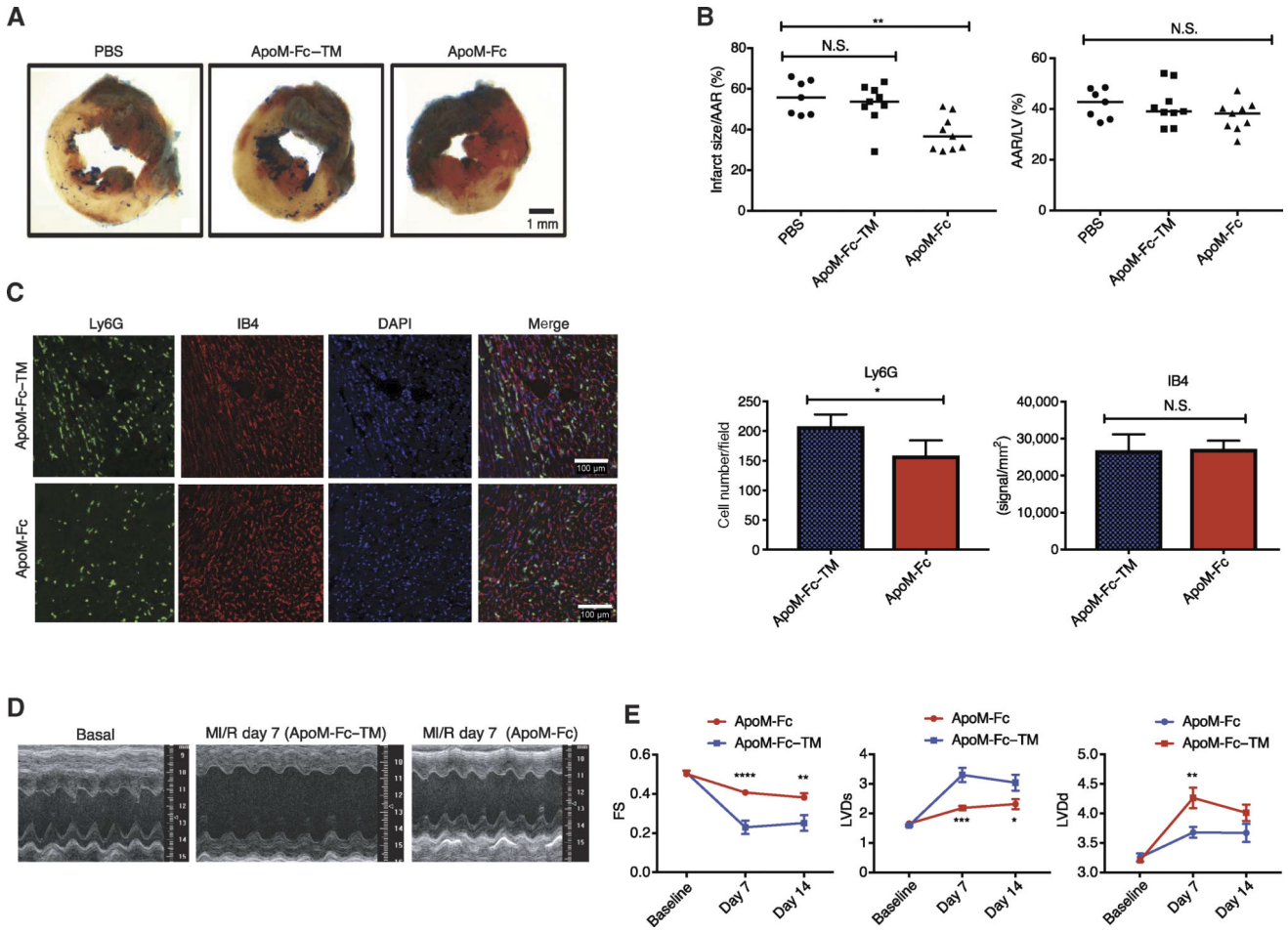

Fig. 6. ApoM-Fc administration attenuates I/R injury in the heart

WT mice were administered PBS ($n = 7$ mice) or either ApoM-Fc (4 mg/kg) ($n = 9$ mice) or ApoM-Fc–TM (4 mg/kg) ($n = 9$ mice) after I/R injury. (**A**) Representative images of left ventricular (LV) slices with Alcian blue and 2,3,5-triphenyltetrazolium chloride (TTC) staining (red), which indicates viable myocardium. (**B**) Quantitative measurement of area at risk (AAR)/LV area and infarct/AAR area was performed in a blinded manner. Median values (one-way nonparametric ANOVA followed by Tukey's test); $^{**}P < 0.01$; N.S. was $P > 0.7$ (left graph) and $P > 0.27$ (ApoM-Fc) and $P > 0.97$ (ApoM-Fc–TM) (right graph). (**C**) Heart sections were stained for Ly6G and IB4, and neutrophils and capillary density were quantified for pixel density. $n = 9$ mice per treatment; mean ± SEM. $P < 0.03$ (left graph) and $P > 0.85$ (right graph), unpaired two-tailed parametric t test. DAPI, 4′,6-diamidino-2-phenylindole. (**D**) Representative images of two-dimensional (2D) guided M-mode echocardiography of the LV at baseline and 7 days after MI/R injury. $n = 6$ mice per treatment. (**E**) LV end-diastolic (LVDd) diameter, LV end-systolic (LVDs) diameter, and fractional shortening (FS) of (D) were measured at the indicated time points after MI/R injury. $n = 6$ mice per treatment; means ± SEM. Two-way ANOVA and Sidak's multiple-comparisons test; $^{*}P < 0.05$; $^{**}P < 0.01$; $^{***}P < 0.005$; $^{****}P < 0.001$.

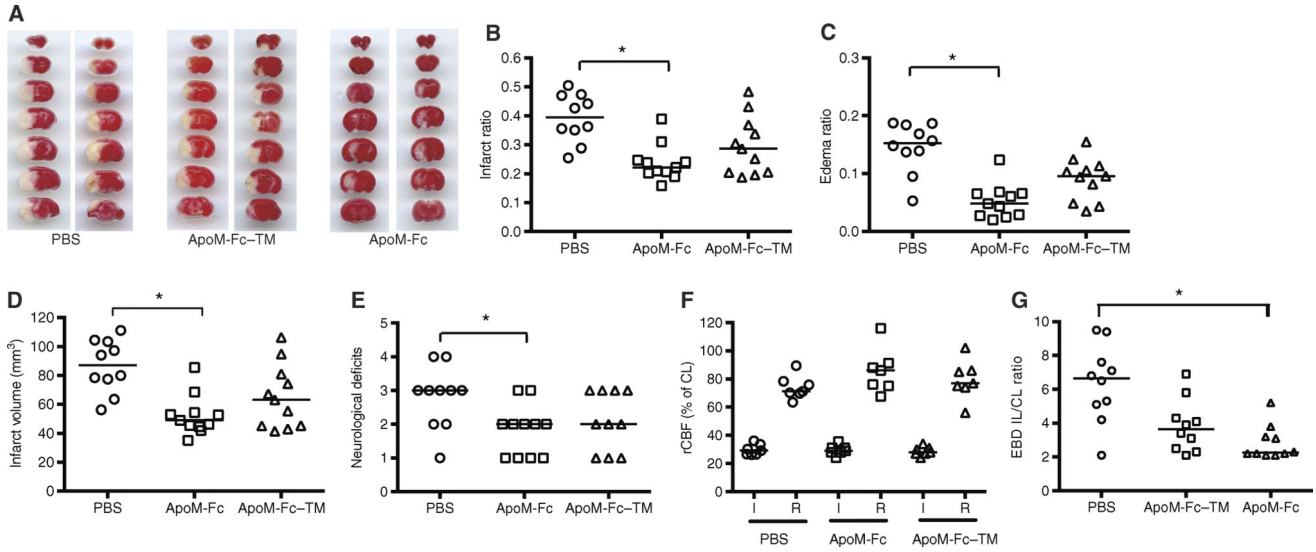

Fig. 7. ApoM-Fc administration attenuates I/R injury in the brain

(**A**) WT mice were subjected to 60 min of focal cerebral ischemia by MCAO. Right after reperfusion, mice received ApoM-Fc (4 mg/kg) (n = 11 mice), ApoM-Fc–TM (4 mg/kg) (n = 11 mice), or PBS (n = 10 mice) by intraperitoneal injection. Representative images of TTC staining of seven, 1-mm-thick brain coronal slices 23 hours after reperfusion. Two mice per group are shown. (**B** and **C**) Infarct (B) and edema (C) ratios were calculated by image analysis and reported as a ratio of the non-ischemic hemisphere. Infarct ratios were corrected for edema. (**D**) Total infarct volume in cubic millimeters, corrected for edema. (**E**) Neurological deficit scores were assessed 23 hours after reperfusion. (**F**) Relative cerebral blood flow (rCBF) in the MCA territory was measured by laser speckle flowmetry during MCAO surgery. rCBF during occlusion (I) and after reperfusion (R) is shown. CL, contralateral. The individual values and the median are shown. *$P < 0.05$ (one-way nonparametric ANOVA followed by Dunn's test). (**G**) Evans blue dye (EBD) extravasation into the brain after MCAO stroke was quantified as described. IL, ipsilateral. Individual values and mean ± SEM are shown from n = 8 to 10 mice per treatment. $P < 0.05$, one-way ANOVA nonparametric test.